OULU 2021
C 774

ACTA UNIVERSITATIS OULUENSIS

Juhani Markus Laitila

EFFECT OF FORCED WELD COOLING ON HIGH-STRENGTH LOW ALLOY STEELS TO INTERPASS TEMPERATURE

UNIVERSITY OF OULU GRADUATE SCHOOL;
UNIVERSITY OF OULU,
FACULTY OF TECHNOLOGY

ACTA UNIVERSITATIS OULUENSIS
C Technica 774

JUHANI MARKUS LAITILA

EFFECT OF FORCED WELD COOLING ON HIGH-STRENGTH LOW ALLOY STEELS TO INTERPASS TEMPERATURE

Academic dissertation to be presented with the assent of the Doctoral Training Committee of Technology and Natural Sciences of the University of Oulu for public defence in the OP auditorium (L10), Linnanmaa, on 1 February 2021, at 10 a.m.

UNIVERSITY OF OULU, OULU 2021

Acta Univ. Oul. C 774, 2021

Supervised by
Professor Jari Larkiola

Reviewed by
Professor Antti Salminen
Doctor Pekka Nevasmaa

Opponents
Professor Antti Salminen
Docent Mika Lohtander

ISBN 978-952-62-2814-3 (Paperback)
ISBN 978-952-62-2815-0 (PDF)

ISSN 0355-3213 (Printed)
ISSN 1796-2226 (Online)

Cover Design
Raimo Ahonen

PUNAMUSTA
TAMPERE 2021

Laitila, Juhani Markus, Effect of forced weld cooling on high-strength low alloy steels to interpass temperature.
University of Oulu Graduate School; University of Oulu, Faculty of Technology
Acta Univ. Oul. C 774, 2021
University of Oulu, P.O. Box 8000, FI-90014 University of Oulu, Finland

Abstract

One of the challenges in welding ultrahigh- and high-strength steels is the effect of limited heat input on the production times. As the cooling times of these steels have to be controlled tightly to achieve the desired weld qualities, such as impact toughness, the allowed heat input is low, which translates to reduced material deposition rates. This means that multipass welding is often required to achieve good weld quality. Because multipass welding is often used, the time spent waiting for the weld to cool to the desired interpass temperature, which is usually 100 °C, is often multiple minutes for each weld pass. The trend so far has been that more efficient welding processes have been developed to maximize the material deposition rates without increasing the heat input. Even with these efforts the use of multipass welding is still required. The use of ultrahigh- or high-strength steels reduces the material cost, allows for lighter and thinner structures while reducing transport costs as well. However, the production cost can negate some of these cost savings because of the wasted time due to the aforementioned problems with multipass welding.

To establish the feasibility of introducing forced cooling to the welding process, the effect of the cooling on the mechanical properties was studied by conducting tensile, impact, and fatigue strength experiments with Gleeble simulated and with welded specimens. Also, the microstructural differences were studied. The tensile properties were improved when forced cooling was used to cool the weld down to the temperature of 100 °C and the impact toughness was also improved or remained unchanged. The cooling also demonstrated that it may have a positive effect on the fatigue strength of the steel. The grain size was usually reduced due to the forced cooling and larger quantities of lower bainite could be seen in some of the experiments. Overall there were no negative effects caused by the forced cooling on the steel.

The external cooling method used was water-cooled copper heat sinks that were placed on top of the steel being welded. This external cooling had the potential to reduce the time it takes for the steel to cool down to 100 °C by 83.6% when 6 mm thick steel was welded. Overall, taking into consideration other processes, such as Setup times, the potential time savings that can be achieved by applying such cooling methods to multipass welding processes is a significant and worthwhile option to consider.

Keywords: arc welding, cooling time, heat-affected zone, high-strength steel, interpass time, multipass welding, production time, ultrahigh-strength steel

Laitila, Juhani Markus, Pakotetun jäähdytyksen vaikutus suurlujuusterästen hitsauksessa.
Oulun yliopiston tutkijakoulu; Oulun yliopisto, Teknillinen tiedekunta
Acta Univ. Oul. C 774, 2021
Oulun yliopisto, PL 8000, 90014 Oulun yliopisto

Tiivistelmä

Hitsausprosesseissa yksi merkittävimmistä ongelmista erikoislujilla teräksillä on saavuttaa riittävän nopeat jäähdytysajat sillä hidas jäähtyminen heikentää hitsin lujuutta. Jäähdytysnopeuksien kasvattaminen vaatii lämmöntuonnin vähentämistä, jolloin hitsipalkojen lukumäärää joudutaan vastaavasti kasvattamaan. Hitsipalkon lämpötila pitää olla esim. 100°C ennen kuin seuraava palko voidaan hitsata päälle. Jäähtyminen saattaa kestää kuitenkin useita minuutteja, jolloin tuotannon tehokkuus kärsii palkojen lukumäärän lisääntyessä. Palkojen määrää on pyritty vähentämään kehittämällä tehokkaampia hitsausprosesseja, mutta siitä huolimatta monipalkohitsausta käytetään yleisesti. Hitsausprosessiin käytetty tehollinen työaika kasvaa jäähtymiseen kuluvan ajan vuoksi ja se kumoaa helposti muutoin optimoidut materiaali- ja kuljetuskustannukset.

Tämän tutkimuksen tarkoituksena oli tutkia nopeutetun eli pakotetun jäähdytyksen vaikutusta erikoislujien terästen mekaanisiin ominaisuuksiin sekä selvittää pakotetun jäähdytyksen aikaansaamiseksi kehitetyn laitteiston suorityskykyä ja vaikutusta tuotannon tehokkuuteen.

Tutkittujen terästen mekaaniset ominaisuudet määritettiin lujuus-, iskusitkeys- ja väsymislujuuskokein. Lisäksi jäähdytyksen vaikutusta teräksen faasirakenteeseen tutkittiin mikrorakennetarkastelujen kautta.

Työssä osoitetaan, että pakotettu jäähdytys paransi hitsien lujuusominaisuuksia kuten myötö- ja murtolujuutta. Lisäksi iskusitkeys kasvoi osalle näytteistä, muiden pysyessä ennallaan. Väsytystestausta tehtiin vain osalle näytteistä mutta niilläkin vaikutus oli positiivinen eli väsymislujuus näytti kasvavan. Teräksen hitsialueen mikrorakenteeseen liittyen, jäähdytys pienensi HAZ-vyöhykkeen raekokoa osassa testeistä, sekä joidenkin terästen kohdalla ala-bainiitin osuus kasvoi selkeästi. Oleellista kokeellisessa osuudessa oli, että jäähdytyksellä ei ollut yhdenkään kokeen kohdalla heikentävää vaikutusta tutkittavan teräksen mekaanisiin ominaisuuksiin. Jäähdytysajat 6,0 mm:n levylle 100°C:een lyhenivät keskimäärin 83,6% käytettäessä hitsin sivulle asetettuja jäähdytysblokkeja. Tämä on merkittävä tekijä tuotannon tehokkuuden kannalta konepajateollisuudessa.

Asiasanat: erikoislujat teräkset, jäähtymisaika, kaarihitsaus, lujat teräkset, monipalkohitsaus, tuotantoaika

“It always seems impossible until it is done.”
Nelson Mandela

Acknowledgements

I would like to thank Business Finland for their financial support as well as Professor Jari Larkiola for arranging the funding and for contributing to my research with his valuable comments. I am also grateful to SSAB for providing the material used in the experiments.

I thank Nyo Tun Tun for conducting most of the tensile strength tests and for preparing the microstructural specimens that I used and Juha Uusitalo for conducting the Gleeble simulations. I would like to thank Jukka Haapio as well for providing me with the cooling data that I used during my research. Furthermore, I would like to thank Lassi-Pekka Keränen for helping me with some of the experiments.

I would like to express my gratitude to Ilpo Alesaarela for preparing my impact toughness specimens. I would also like to extend my thanks to the workshop personnel at the University of Oulu for preparing my specimens for me as well as manufacturing the heat sinks that were used in the experiment. Furthermore, I would like thank David Porter for his valuable contribution to my articles.

I am also grateful to my coworkers Heikki Pirkola, Jouko Heikkala, and Jyri Porter for their help during my research.

My infinite gratitude goes out to my wife who took care of our son and home during my research and who gave me hope on multiple occasions during the process when I felt like quitting.

28.11.2020 Juhani Markus Laitila

List of abbreviations and symbols

°	Degree
°C	Celsius
µm	Micrometer
A_1	Temperature in which austenite starts to form
A_5	Elongation to fracture
Al	Aluminum
ANOVA	Analysis of variance
C	Carbon
CEV	Carbon equivalent value
CGHAZ	Coarse grain heat-affected zone
CMT	Cold metal transfer
CO_2	Carbon dioxide
d	Plate thickness
F_2	Shape factor for two-dimensional heat flow based on form of weld
F_3	Shape factor for three-dimensional heat flow based on form of weld
FCAW	Flux-cored arc welding
FCFT	Forced cooling finish temperature
FESEM	Field emission scanning electron microscope
FGHAZ	Fine grain heat-affected zone
GMAW	Gas metal arc welding
GMAW-P	Pulsed gas metal arc welding
HAZ	Heat affected zone
HSLA	High-strength low-alloy
Hz	Hertz
I	Welding current
ICCGHAZ	Intercritically reheated coarse grain heat-affected zone
ICHAZ	Intercritical heat affected zone
J	Joule
k	Thermal efficiency
kJ	Kilojoule
kN	Kilonewton
l/min	Liters per minute
LBZ	Local brittle zone
MA-const.	Martensite-austenite constituent
MAG	Metal active gas

Max	Maximum
MIG	Metal inert gas
Min	Minimum
mm	Millimeter
Mn	Manganese
Mo	Molybdenum
MPa	Megapascal
M_s	Temperature at which martensite begins to form
Nb	Niobium
P	Phosphorus
PAW	Plasma arc welding
p-value	Probability value
Q	Heat input
R	Radius
R_m	Tensile strength
$R_{p0.2}$	Yield strength at 0.2% elongation
s	Seconds
S	Sulfur
SAW	Submerged-arc welding
SCHAZ	Sub-critical HAZ
SEI	Secondary electron microscope
Si	Silicon
SMAW	Shielded metal arc welding
T_0	Working temperature
$t_{5/1}$	Cooling time from 500 to 100°C
$t_{8/1}$	Cooling time from 800 to 100°C
$t_{8/5}$	Cooling time from 800 to 500°C
Ti	Titanium
U	Voltage
UCGHAZ	unaltered CGHAZ
V	Volt
v	Travel speed
V	Vanadium
wt.%	Weight volume fraction percentage
Y/T-ratio	Yield-to-tensile ratio

List of original publications

This thesis is based on the following publications, which are referred throughout the text by their Roman numerals:

I Laitila, J., Larkiola, J., & Porter, D. (2017). Effect of forced cooling on the tensile properties and impact toughness of the coarse-grained heat-affected zone of a high-strength structural steel. *Welding in the World*, *62*(1), 79–85. https://doi.org/10.1007/s40194-017-0532-z

II Laitila, J., Larkiola, J., & Porter, D. (2018). Effect of forced cooling after welding on CGHAZ mechanical properties of a martensitic steel. *Welding in the World*, *62*(6), 1247–1254. https://doi.org/10.1007/s40194-018-0617-3

III Laitila, J., Larkiola, J., & Porter, D. (2019). Effect of heat sinks on cooling time to weld interpass temperature. *MATEC Web of Conferences*, *269*, 01007. https://doi.org/10.1051/matecconf/201926901007

IV Laitila, J., & Larkiola, J. (2019). Effect of enhanced cooling on mechanical properties of a multipass welded martensitic steel. *Welding in the World*, *63*(3), 637–646. https://doi.org/10.1007/s40194-018-00689-7

V Laitila, J., Keränen, L. & Larkiola, J. (2020). Effect of enhanced weld cooling on the mechanical properties of a structural steel with a yield strength of 700 MPa. *SN Applied Sciences, 2*, 1888. https://doi.org/10.1007/s42452-020-03695-x

Contents

1 Introduction

1.1 Background

The demand for stronger and lighter structures has created a demand for ultrahigh- and high-strength steels. For example, if steel of grade S1100QL is used to replace S355 in a structure, the wall thickness can be reduced by up to 73%. In addition, if the wall thickness is thin enough for single-pass welding, the filler material consumption can be significantly reduced. The reduction in wall thickness can also reduce the potential bending and cutting costs [1–5].

However, the ultrahigh- and high-strength steels are more challenging to weld than S355. Heat input must be more strictly limited not only for the reasons involving factors caused by thermal expansion but for microstructural reasons as well [6]. The heat input of welding produces a heat-affected zone (HAZ), which is detrimental to the mechanical properties of the steel [7]. How detrimental the HAZ is to the welded joint is dependent on the width of the HAZ and on the microstructure in the zone, which is produced by the thermocycle caused by welding.

The cooling cycle and the peak temperature have a significant effect on the grain size and on the type of the microstructure of the steel in the HAZ. Faster cooling rates produce a smaller grain size, which is beneficial to the impact toughness and strength of the steel. Furthermore, with faster cooling rates to sufficiently low temperatures, the microstructure of the HAZ can become martensitic or bainitic, which gives the HAZ high tensile and yield strength levels. If the microstructure is martensitic the impact toughness tends to be lower than with bainite. However, martensite generally has a higher tensile strength than bainite, unless the bainite produced is lower bainite, which can have similar tensile properties to that of martensite while also having superior impact toughness.

There are a few different ways to achieve sufficiently low heat input when welding ultrahigh- or high-strength steels, such as using laser-based welding technologies or by reducing the welding energy when using arc welding methods. However, more advanced welding technologies are expensive compared to arc welding technologies and sometimes also require strict tolerances for the weld seam preparation.

If the welding energy is reduced when using a metal active gas (MAG) welding method, the number of weld passes increases, which means that production time

greatly increases as it can take minutes for the steel to cool down to interpass temperature, in addition to the increased welding time. Therefore, introducing external cooling to the process could be beneficial as it reduces the time it takes for the weld to cool down to interpass temperature. However, it is unknown whether the cooling will have a beneficial, neutral or negative effect on the mechanical properties of the joint. If the cooling does not have a negative effect on the weld and the cooling time reduction is sufficiently significant, cooling should be introduced to the welding process when the process requires multiple weld passes. However, the cooling methods currently used in the industry have low cooling potentials, are expensive or are not suitable for beam structures.

1.2 Objectives and structure of the research

The first objective of this research is to study the effects of external cooling on the mechanical properties of the multipass welded joint, when the cooling is applied all the way to interpass temperature. The second objective is to establish how effective heat sink technology is when heat sinks are placed on top of the weld instead of on the bottom of the weld. By placing the heat sinks on the top of the weld, more challenging weld applications could adapt external cooling. Special focus is given to beam structures, because they are impossible to cool in practice with heat sinks that are placed below the weld. The roadmap for the research is shown in Fig. 1.

Hypotheses:

- As the limit to which the steel is cooled rapidly decreases, the impact toughness and tensile strength of the HAZ increases
- By placing heat sinks on top of the weld, a significant amount of wasted time can be eliminated from the welding process
- The cooling provided by the heat sinks will also produce a weld joint with superior mechanical properties
- Residual stresses in the steel will decrease and hence fatigue strength will increase
- The heat sinks will limit thermal expansion significantly

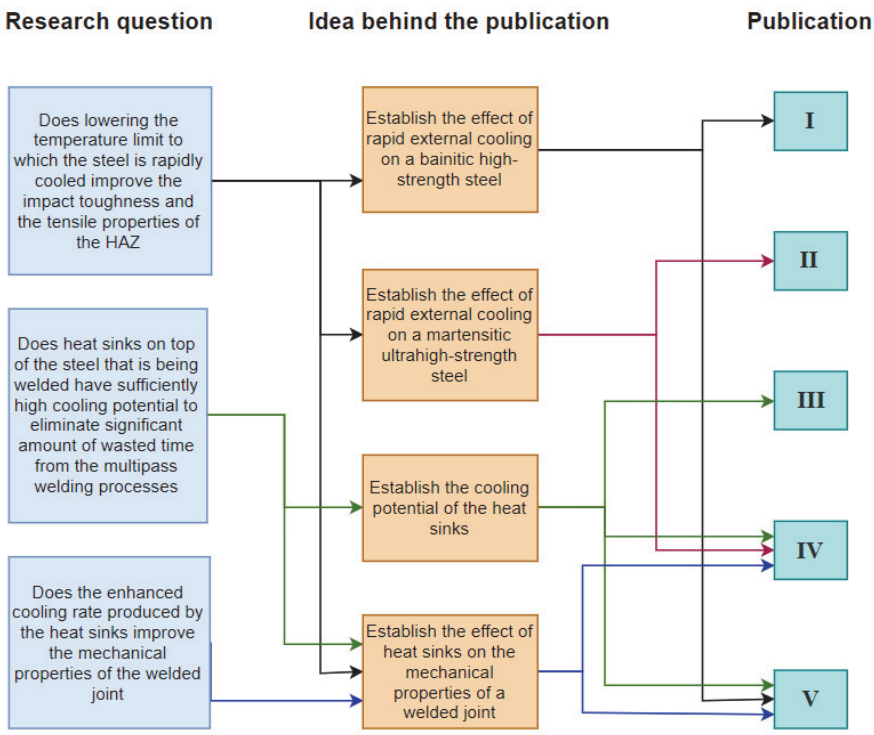

Fig. 1. Roadmap for the research.

2 Theoretical background

2.1 Microstructures of advanced steels

The superior mechanical properties of the high- and ultrahigh-strength steels are caused mainly by bainite and martensite that form in temperatures below 500 °C [8]. These microstructures have much higher tensile properties compared to other microstructures that can be present in the steel, such as ferrite, austenite, pearlite or cementite. However, low alloy steels with higher strengths can have lower impact toughness than mild steels because of the presence of martensite, which tends to be brittle unless the carbon content of the steel is low and the grain size is relatively small as well. Other factors that also affect the impact toughness of the steel are the martensite-austenite constituents (MA-constituents), carbides, and grain size. MA-constituents tend to have a negative effect on the impact toughness of the steel, especially when they are necklaced. The carbides and grain size tend to affect the toughness as well: the coarser they are, the more brittle the steel will be.

2.1.1 Upper and lower-bainite

Bainite is the main microstructure of many steels that have a tensile strength of around 700 MPa. Often the steels that have a mainly bainitic structure have a significant amount of ferrite in them as well, and they are often labelled as ferritic-bainitic steels that have a tensile strength between 450 and 900 MPa. Ferritic-bainitic steels usually have relatively good weldability, high impact toughness, and high tensile strength. Furthermore, bainite can still be found in steels with a tensile strength of above 900 MPa [9].

Bainite has a distinct plate- or lath-like structure and forms in temperatures between of 550 and 250 °C depending on the steel, and it can be divided into upper and lower bainite. In temperatures above 400 °C, the bainite that forms is upper bainite and it has lower tensile strength properties than lower bainite. However, it is usually the dominant bainite in ferritic-bainitic steels. The formation mechanism for upper and lower bainite can be seen in Fig. 2. The main difference between upper and lower bainite is that upper bainite has cementite precipitations only between the plates and lower bainite has them in between lathes as well as inside the plates. Examples of the microstructures can be seen in Figs. 3 and 4. Lower

bainite forms in temperatures between 400 °C and 250 °C. However, it can sometimes form in temperatures that are below M_s as well [10–12].

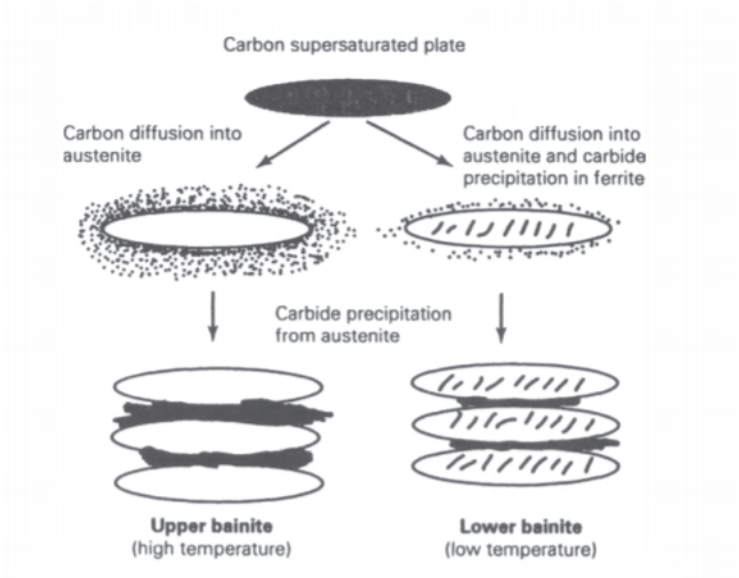

Fig. 2. Bainite transformation schematic (Reprinted, with permission, from [10] © 2006 Elsevier).

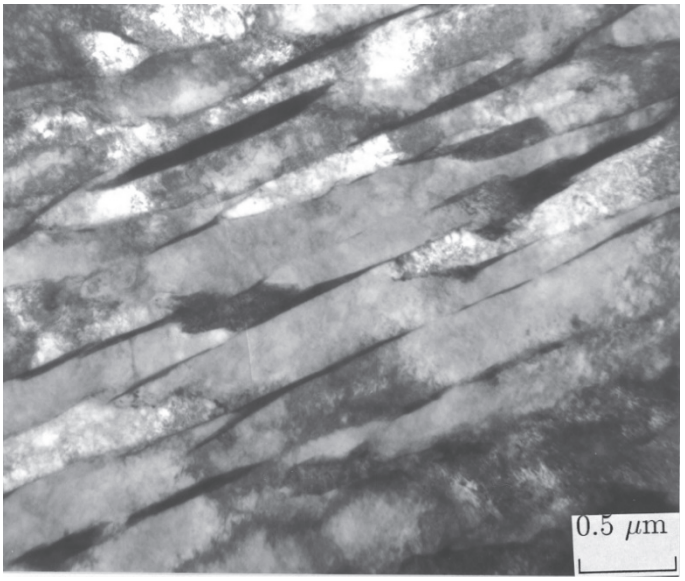

Fig. 3. Microstructure of upper bainite (Reprinted, with permission, from [13] © 1996 The Institute of Materials).

In addition to the transformation temperatures, the cooling rate plays an important part in the formation of bainite. The cooling rate of the steel when bainite forms is faster than it is when pearlite forms, but slower than what is required for martensite formation. Furthermore, lower bainite is hard to distinguish from tempered martensite due to their similarities. Both lower bainite and tempered martensite have cementite precipitates in them, but the difference is that in lower bainite these precipitates are oriented only in one direction. Lower bainite precipitates are in parallel arrays in 60° orientation to the bainite plates and in tempered martensite they are in Widmanstätten arrays [10,14].

The carbides in lower bainite are finer and the density of dislocations is higher than in upper bainite, which leads to the superior impact toughness and tensile strength of lower bainite when compared to upper bainite. In some cases, the tensile strength of lower bainite can be like that of martensite while also having higher impact toughness properties [11,12,14–19].

Fig. 4. Microstructure of lower bainite (Reprinted, with permission, from [13] © 1996 The Institute of Materials).

2.1.2 Martensite

Martensite is the main microstructure in many ultrahigh-strength steels due to it having very high tensile strength properties. However, martensite tends to be quite brittle compared to microstructures such as bainite and austenite, but it generally has the highest tensile strength among all the possible microstructures in ultrahigh-strength steels. To achieve a martensitic microstructure, the steel has to be cooled rapidly from high temperatures in which the steel is in austenite form to low temperatures. This can be achieved by quenching. In fact, martensite requires the fastest cooling rate of all of the microstructures. If the cooling rate is not fast enough the steel can transform, for example, into bainite, ferrite, cementite or

pearlite. The required cooling rate depends on the alloying elements. For example, if the steel has high amounts of alloying elements that stabilize the austenite, the cooling rate required for martensite to form can be quite slow [20].

Martensite is a crystalline structure that is formed without diffusion. In steels, martensite is a supersaturated solution of carbon in ferritic iron. Carbon content actually affects the formation and type of martensite that is produced in the steel. Different microstructural examples of lath martensite can be seen in Fig. 5. Lath martensite is the dominant type of martensite found in low carbon steels. Other than the type of martensite that is produced, the carbon also affects the temperature in which martensite forms as well as how tough the martensite is. For example, in steel that has a carbon content of around 0.2%, martensite can already begin to form in temperatures as high as 500 °C [20].

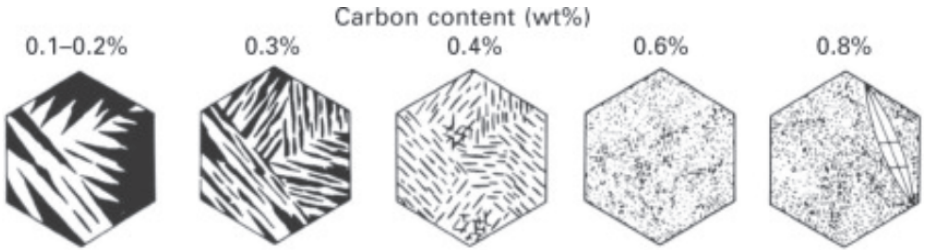

Fig. 5. Lath martensite microstructure by carbon content (Reprinted, with permission, from [21] © 2012 Woodhead Publishing Limited).

2.2 Welding ultrahigh- and high-strength steels

Welding ultrahigh- and high-strength steels demands the use of low heat input or the mechanical properties of the joint will suffer greatly. Manufacturers often provide guidelines for the maximum allowed heat input as can be seen in Figs. 6, 7 and 8.

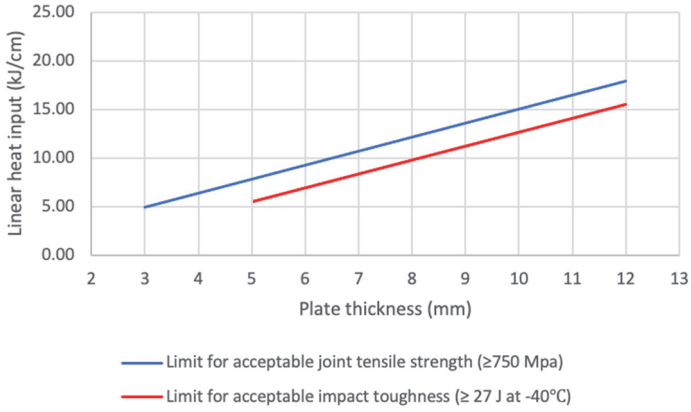

Fig. 6. Maximum allowed heat input for grade 700 steel (Redrawn from [22]).

One of the reasons behind providing maximum allowed heat input guidelines is that it is directly related to the time it takes for the weld to cool down from 800 to 500 °C ($t_{8/5}$), during which most of the microstructural changes take place [25]. Manufacturers provide recommended $t_{8/5}$ times as well, and it is possible to derive the allowed heat input from these cooling times by using readymade calculator applications such as WeldCalc or by calculating it by hand. It is relatively easy to calculate the $t_{8/5}$ when the welding parameters are known. Usually the recommended $t_{8/5}$ times are between 4 and 20 seconds and the higher the strength grade of the steel is, the shorter the recommend $t_{8/5}$ tends to be [22,24,25].

The heat input of a weld can be calculated (in units of kJ/mm) by using equation [26]

$$Q = k \times I \times \frac{U}{v} \times 10^{-3}. \quad (1)$$

The symbols used in the Equation 1 are given in Table 1.

Table 1. Explanation of symbols used in Equation 1 [26].

Symbol	Explanation
Q	Heat input (kJ/mm)
k	Thermal efficiency (0.8 for GMAW / 1.0 for SAW)
U	Arc voltage (V)
I	Welding current (A)
v	Travel speed (mm/s)

After the heat input is known and depending on whether the cooling process is 2D or 3D, the cooling time from 800 °C to 500 °C ($t_{8/5}$) can be calculated by using equation [27]

$$t_{8/5} = (4300 - 4.3T_0) \times 10^5 \times \frac{Q^2}{d^2} \times \left[\left(\frac{1}{500-T_0}\right)^2 - \left(\frac{1}{800-T_0}\right)^2\right] \times F_2 \quad (2)$$

or equation [27]

$$t_{8/5} = (6700 - 5T_0) \times Q \times \left[\left(\frac{1}{500-T_0}\right) - \left(\frac{1}{800-T_0}\right)\right] \times F_3. \quad (3)$$

The symbols used in the Equations 2 and 3 are explained in Table 2.

Table 2. Explanation of symbols used in Equations 2 and 3 [27].

Symbol	Explanation
d	Plate thickness (mm)
Q	Heat input (kJ/mm)
T_0	Working temperature (°C)
F_2	Shape factor for two-dimensional heat flow based on form of weld (Butt weld =0.9)
F_3	Shape factor for three-dimensional heat flow based on form of weld (Butt weld =0.9)

The working temperature, which is same as interpass temperature in multipass welding, has a significant effect on the $t_{8/5}$, particularly in the case of thin plates and 2-dimensional heat flow. It is one of the reasons why the interpass temperature should be as low as possible. An example of how the T_0 effects the $t_{8/5}$ can be seen in Table 3.

Table 3. Calculated cooling times with heat input of 0.75 kJ/mm and 8 mm plate (Butt weld, MAG).

T_0 (°C)	$t_{8/5}$
20	8.87 s
100	12.7 s
200	22.3 s
300	49.3 s

Furthermore, the effect of the T_0 on the recommended maximum heat input of one manufacturer's steel can be seen in Figs. 7 and 8. The steels in these figures are the same, the only difference between the figures is that in Fig. 7 the T_0 is 20 °C and in Fig. 8 it is 100 °C.

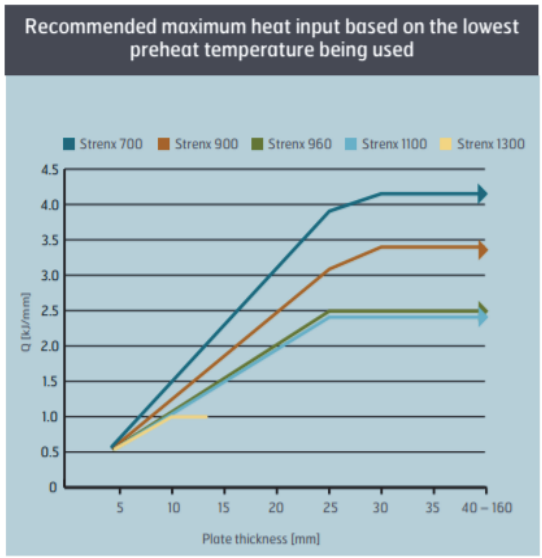

Fig. 7. Maximum heat input allowed for grade 700 to 1300 steels according to one manufacturer (Reprinted, with permission, from [25] © 2018 SSAB).

Fig. 8. Maximum allowed heat input for grade 700–1300 steels when interpass temperature is 100 °C (Reprinted, with permission, from [25] © 2018 SSAB).

From a production point of view, when these steels are welded, a T_0 of 20 °C would be ideal as it would allow a significantly higher heat input, which translates to a higher deposition rate of weld metal. However, as a general rule of thumb, it can be said that when ultrahigh- or high-strength steels are welded and the material thickness equals or is greater than 6 mm, multipass welding is often required. In fact, if a matching weld is desired, weld thickness of 6 mm could require up to three weld passes, which leads to a highly inefficient production process. Between the weld passes the welders or robots must wait for the weld to cool down back to a T_0 of 100 °C, which usually takes a significant amount of time and leads to increased production costs [24].

Even though the allowable interpass temperature can reach as high as 300 °C [28–30], the ideal interpass temperature is often around 100 °C and it is usually recommended by manufacturers. For example, research conducted by Wang et al. [31] has demonstrated that an interpass temperature of around 100 °C produces a joint with the best mechanical properties. Furthermore, other research conducted by Peng et al. [32] demonstrated that an interpass temperature of 80 °C with 690 MPa grade high-strength low-alloy (HSLA) steel produced superior mechanical properties when compared to higher interpass temperatures.

In addition, the welds of ultrahigh- and high-strength steels are very sensitive to hydrogen cracking, meaning special attention has to be paid to the purity and hydrogen scale of the filler material, as well as to the cleanliness of the weld seam prior to welding, and to the shielding gas. Furthermore, the weld cannot be quenched right away after welding since it would cause unfavorable microstructural changes in the weld as well as hydrogen cracking, as the hydrogen does need some time to escape the weld. However, at lower temperatures quenching could be used as per the previous point of view, but in multipass welding application this would still remain highly undesirable because of the impurities left in the weld seam caused by the quenching process.

2.2.1 Welding processes

Ultrahigh- and high-strength steels are usually welded by using arc, resistance or laser welding. Also, the hybrid form of arc and laser welding is sometimes used. Resistance and laser welding methods are often used in the automotive industry and in other applications where the material is relatively thin [33]. When laser welding is used, the seam tolerance requirements are very strict and the $t_{8/5}$ of the weld can be too short, which leads to a brittle joint [34,35]. When structural beam

structures or pipes made from ultrahigh- or high-strength steel are welded, arc welding methods are usually used. Therefore, this work will focus on arc welding processes. Furthermore, the welding guidelines provided by the manufacturers usually focus on arc welding methods as well [22,25].

Arc welding traditionally consists of the following welding processes: gas metal arc welding (GMAW), gas tungsten arc welding (GTAW), plasma arc welding (PAW), submerged arc welding (SAW), flux cored arc welding (FCAW), and shielded metal arc welding (SMAW) [33]. However, the hybrid of laser and GMAW can be thought of as being part of the arc welding category [34].

From the traditional arc welding methods, SAW and GMAW are the most commonly used for ultrahigh- and high-strength steels when pipes or structures such as trusses are being welded. For example, SAW has the highest arc efficiency of the arc welding methods and is a popular choice for automated welding applications when thicker materials are used in structures such as pipes. GMAW on the other hand is a very versatile welding process and can be used for different material thicknesses, multiple different joint geometries, and can be used in tandem with welding robots to weld all kinds of structures [33].

As arc welding methods have a high heat input, the welding equipment manufacturers have been trying to develop more advanced versions of GMAW that have reduced heat input. This has been achieved by applying a different version of pulsed GMAW (P-GMAW). By pulsing the current or wire feed or both, the heat input applied by the process can be minimized without reducing the material deposition rate. Different manufacturers have different terms for this, such as cold metal transfer (CMT), which was invented by Fronius [33,36]. Furthermore, manufacturers also try to reduce heat input or increase material deposition rate without increasing heat input by adding cold wires to the welding process. For example, ESAB has developed the ICE process for SAW welding. In the ICE process, three welding wires are fed into the weld, but only one of them is feeding a current to the weld and thereby the material deposition rate is maximized [37].

2.2.2 Heat-affected zone

The heat input produced by the welding arc causes microstructural changes in the weld that are detrimental to the welded joint. However, the weld is not the weakest area of the weld, but HAZ is. HAZ can be divided into different sub-zones that can be also seen in Fig. 9. The sub-zones are produced by different peak temperatures, hence their location is based on the distance from the fusion line. Coarse-grained

heat-affected zone (CGHAZ) is closest to the fusion line and has the largest grain size, as the name implies. CGHAZ is usually caused by a peak temperature of 1350 °C [38,39]. The zone following CGHAZ is fine-grain HAZ (FGHAZ) that is produced by peak temperatures that are above 850 °C. After FGHAZ, the next zone is intercritical HAZ (ICHAZ), which is produced by temperatures above 750 °C in which austenite begins to form (A_1). The last zone with the lowest peak temperature is sub-critical HAZ (SCHAZ), which is caused by temperatures that are below the A_1 temperature but above 500 °C. Furthermore, in multipass welding there are different combinations of HAZ, such as intercritically reheated CGHAZ (ICCGHAZ), these combinations and their names can be seen in part b of Fig. 1 [1,40–42].

The detrimental effect of these zones can be divided into two categories from the point of view of their mechanical properties. The zone can have a softening effect and thereby lower the strength of the steel. For example, FGHAZ, ICHAZ and SCHAZ are zones in which the tensile strength of the steel tends to decrease. The zones that have inferior impact toughness properties are called local brittle zones (LBZ). The ICCGHAZ, CGHAZ, ICHAZ or the unaltered CGHAZ (UCGHAZ) are usually brittle zones of the weld, meaning they are part of the LBZ term. If multipass welding is used, it is likely that ICCGHAZ will be the primary LBZ. Furthermore, ICCGHAZ tends to have significantly more MA-constituents and they are larger in size than in other sub-zones of HAZ [40–42].

Furthermore, ICHAZ can have both inferior tensile strength and impact toughness in relation to the base material. Unlike FGHAZ which tends to have high impact toughness due to the softening it undergoes, which also causes the lower tensile properties [42].

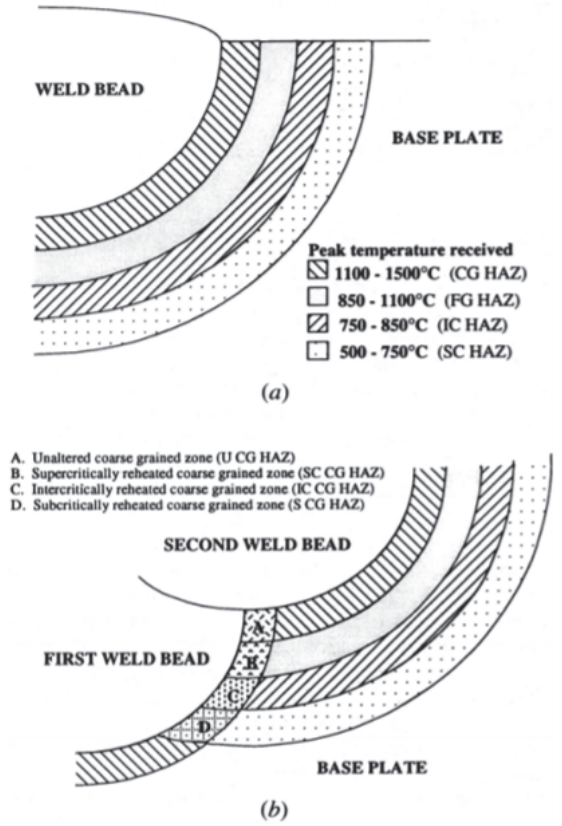

Fig. 9. Different heat-affected zones of (a) single-pass and (b) multipass-welds (Reprinted, with permission, from [43] © 1994 The Minerals, Metals and Materials Society, and ASM International).

Every weld pass after the initial weld pass gives birth to new ICCGHAZ and UCGHAZ, which means the number of LBZs increases as the number of weld passes increases. This means that, probabilistically, the multipass weld becomes more susceptible to fractures, which is detrimental to the quality of the weld.

2.2.3 Cooling of the weld

Applying external cooling to the steel being welded has multiple potential benefits to the welded joint. Even steels with low tensile strength classification such as 316L, can benefit from external cooling in the form of reduced residual stresses [44].

Furthermore, when multipass welding has been used for high-strength steels, pressurized air has been used to reduce the time it takes for the weld to cool down to the desired interpass temperature [45]. Distortions caused by the welding process can be minimized by applying external cooling on the metal as well, especially when sheet metals are being welded [46].

The cooling methods that are used can be divided into the following categories: heat sinks, solid CO_2, liquid nitrogen, liquid argon or pressurized air. Out of these categories pressurized air has the lowest cooling potential while the heat sink technology along with solid CO_2 have high cooling potentials, and liquid nitrogen and argon are in the middle [46].

Out of these cooling methods, pressurized air is the easiest to apply and the equipment is relatively cheap, but the cooling potential is very poor. For example, cryogenic cooling with solid CO_2 has 100 times greater cooling potential [46]. Meaning that the cooling rates that can be achieved with pressurized air are not that great. However, every cooling method other than heat sinks and pressurized air consumes the coolant in the process, meaning that they are not feasible, economic or environmentally friendly choices for cooling a weld in truss structures where the material thickness is greater than in sheet metal applications.

For prolonged cooling in which cooling potential is important, the heat sink makes the most sense. However, the heat sinks that have been used in the past have always been placed under the steel being welded, which is also not possible in truss applications in which the structures that are being welded are often tubular. Furthermore, the focus of previous studies has usually been the reduction of distortions and buckling that can be caused by the heat produced by the welding process.

2.2.4 Residual stresses and fatigue

Residual stresses are always present in welded structures as the thermocycle caused by the welding process will give birth to residual stresses in the steel by thermal expansion as the steel becomes warmer and by thermal reduction when it cools. The quantity of residual stresses in the welded joint has an impact on its fracture resistance and fatigue strength. Therefore it is important to minimize the residual stresses caused by the heat input of the welding process. Besides the effects of residual stress on the aforementioned mechanical properties, it can also cause physical deformations and have a negative effect on the corrosion resistance of the material that is being welded [47].

One way to minimize residual stress that is caused by the welding process is to introduce external cooling. In a study conducted by Jiang et al. [44], copper heat sinks were placed under the steel sheet that was being welded. It was found that the heat sinks reduced the residual stress by 20%. From the point of view of fatigue strength, this translates to a significant improvement as the fatigue strength of the steel correlates strongly with the residual stress.

If the welded joint is located in a structure that experiences dynamic loads, fatigue strength becomes an extremely important factor. When a structure is exposed to dynamic load, the crack propagation is usually caused by fatigue [48,49]. Furthermore, forecasting the fatigue strength of any given joint is difficult as it is a relatively independent parameter [50]. Many different factors, such as local weld bead geometry, have an effect on the fatigue strength of the steel, but one of the easiest factors to control is residual stress. As proved by Jiang et al. [44], reducing heat input or using more sophisticated welding equipment, such as laser welding, is not the only way to achieve lower residual stress in the welded joint. Furthermore, introducing external cooling to the welding process is significantly more cost effective than using post-weld heat treatments to eliminate residual stress.

3 Experiments

The statistical analysis used to analyze the impact toughness, fatigue, tensile and yield strength results is one-way analysis of variance (ANOVA). This test is used to compare various groups against each other to determine whether the groups are different from each other in respect of one factor. In every analysis the confidence interval used is 95%, which means that if the p-value is lower than 0.05, there is a 95% probability that there is a statistically significant difference between the compared sample groups.

3.1 Gleeble experiments for 700 MC and 960 QL CGHAZ

The commercial grade steels used in the experiments in which CGHAZ was simulated with Gleeble had tensile strengths of 700 and 960 MPa. The chemical composition of the steels can be seen in Tables 4 and 5. The chemical composition of the steel seen in Table 4 had a yield strength ($R_{p0.2}$) of 700 MPa, a tensile strength (R_m) in the range of 750–950 MPa, an elongation to fracture (A_5) of at least 13%, and a specified minimum impact strength of 27 Joules at -40 °C. The steel was manufactured by hot-rolling and it had a bainitic-ferritic microstructure while having the carbon equivalent (CEV) of 0.37. [51, Paper I] The steel seen in Table 5 was manufactured by quenching and had a martensitic-ferritic microstructure. This steel had a minimum specified yield strength ($R_{p0.2}$) of 960 MPa, a tensile strength (R_m) in the range 980–1150 MPa, an elongation to fracture (A) of at least 12%, a specified minimum impact strength of 40 Joules at -40 °C, and a CEV of 0.58 [52,Paper II]. The CEV values were formulated by using the equation [51,52]

$$\mathrm{CEV} = \mathrm{C} + \frac{\mathrm{Mn}}{6} + \frac{\mathrm{Cr+Mo+V}}{5} + \frac{\mathrm{Cu+Ni}}{15}, \tag{4}$$

where symbols represent the steel alloy content (in wt.%) of corresponding elements.

Table 4. Chemical composition of the 700 MC, wt.% [51] (Reprinted, with permission, from Paper I © 2017 International Institute of Welding).

C max	Si max	Mn max	P max	S max	Al min.
0.10	0.20	2.10	0.020	0.010	0.015

Table 5. Chemical composition of 960 QL (wt.% max) [52] (Reprinted, with permission, from Paper II © 2018 International Institute of Welding).

C	Si	Mn	P	S	Cr	Cu	Ni	Mo	B
0.20	0.50	1.60	0.020	0.010	0.80	0.30	2.00	0.70	0.005

Both materials underwent the same Gleeble simulation with the same thermocycle parameters. The heating rate that was used in the experiment was 400 °C/s and the specimens had a peak temperature of 1350 °C in which the specimens were held for one second. After they were soaked for one second at peak temperature, they were rapidly cooled down to 500, 400, 300, 200 or 100 °C with two different cooling rates of 50 and 15 °C/s. After hitting the lower limit of the rapid cooling, they were cooled to room temperature with cooling rates that are similar to air cooling. In this context, air cooling means the cooling rate that a normal welded seam would undergo. The air-cooling rates used in the simulations are rates that were taken from the thermocouple measurement of a real fillet weld done by Jukka Haapio in Kemppi Oy's laboratory. The heat input in that experiment was 1.5 kJ/mm, travel speed was 336 mm/min, the material thickness was 8 mm and the length of the weld was 165 mm [Papers I–II].

The air cooling rates can be seen in the Table 6 and examples of two different cooling cycles including the forced cooling and air cooling can be seen in the Fig. 10.

Table 6. Simulated air-cooling rates (Reprinted, with permission, from Paper I © 2017 International Institute of Welding).

Temperature range (°C)	Cooling rate (°C/s)
500–450	7.10
450–400	5.00
400–350	3.85
350–300	2.77
300–250	2.00
250–200	1.28
200–150	0.69
150–100	0.29

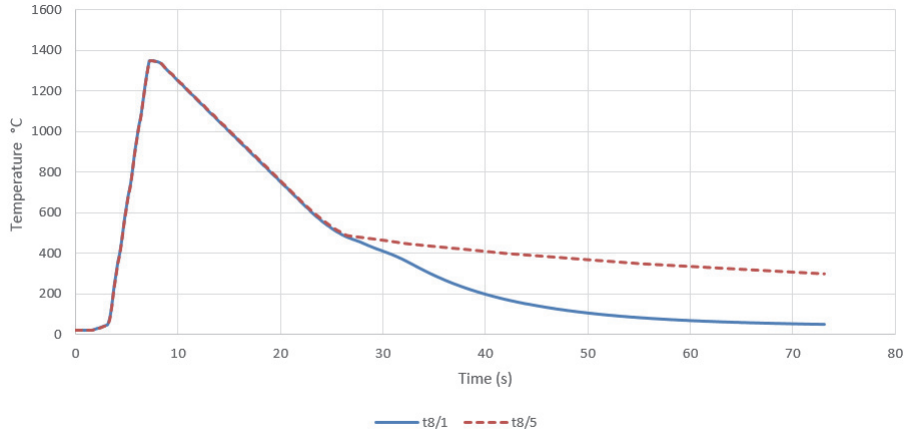

Fig. 10. Thermal cycle with cooling rate of 50 °C/s down to 500 and 100 °C/s (Reprinted, with permission, from Paper I © 2017 International Institute of Welding).

Two different types of specimens of each material were used for the Gleeble simulation, the first being tensile strength specimens, which had the dimensions of 120xØ6 mm in the case of bainitic steel and 160xØ10 mm in the case of martensitic steel before the Gleeble simulation. After the simulation the tensile strength specimens were machined. The bainitic steel was machined to have the nominal diameter of 4 mm and parallel length of 15 mm. The martensitic steel was machined to have the nominal diameter of 6 mm and parallel length of 15 mm [Papers I–II].

Impact toughness specimens were the other kind of specimens prepared. These were Charpy V-notch specimens that were fabricated according to ISO 148-1 for both materials. The size of the specimen used was 5x10x55 mm and the V-notch was added after the Gleeble simulation [Papers I–II].

The tensile, yield, and elongation testing was carried out with a Zwick 100kN testing machine and three individual specimens were used per simulated parameter. Furthermore, three specimens were also used in the Charpy V-notch tests. These tests were carried out in -40 °C and the ductile fracture percentages were evaluated visually according to ISO 148-1 [Papers I–II].

3.2 Cooling potential experiment with heat sinks

The cooling potential welding experiment was carried out by utilizing a Kemppi Pro MIG 500 and a Motoman-yasnac RX robot on a basic S355 structural steel.

The welding parameters can be seen in Table 7 and the welding jig in Fig. 11 [Paper III].

Table 7. Welding parameters used in the experiment (Reprinted [adapted] under CC BY 4.0 license from Paper III © 2019 Authors).

Parameter	Value
Current	167 A
Voltage	22.7 V
Travel speed	220 mm/min
Angle of the weld torch	15°
Welding technique	Push
Wire feed	9.8 m/min (Autorod 12.51, Ø0.8 mm)
Welding energy	1.03 kJ/mm
Heat input	0.83 kJ/mm
Gas flow rate	16 l/min (Mison 25)
Working temperature	21 °C
Weld passes	1

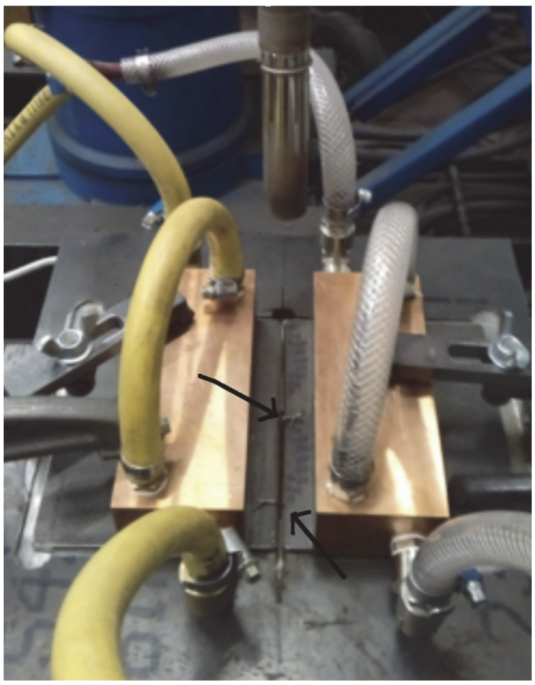

Fig. 11. Weld setup with two thermoelements and cooling blocks (Reprinted [adapted] under CC BY 4.0 license from Paper III © 2019 Authors).

The steel pieces used for the welding experiment had the dimensions of 120x145x6 mm of which 145 mm was the length of the weld. The joint geometry chosen for the experiment was a v-groove butt-weld joint with a groove angle of 50 degrees, a root face of 1 mm, and a root gap of 1 mm, as can be seen in Fig. 12 [Paper III].

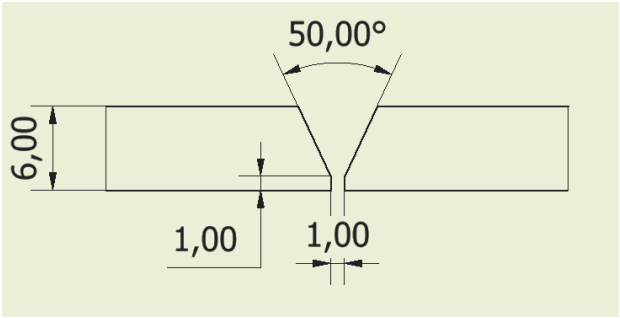

Fig. 12. Joint dimensions (mm) (Reprinted under CC BY 4.0 license from Paper III © 2019 Authors).

The potential of the external cooling which was measured in the experiment was provided by water cooled copper blocks that were placed on top of the steel as can be seen in Fig. 11. The parameters and dimensions of the cooling blocks can be seen in Table 8 and Fig. 13 [Paper III].

Table 8. Copper (C110) cooling block parameters (Reprinted [adapted] under CC BY 4.0 license from Paper III © 2019 Authors).

Parameter	Value
Copper block length	150 mm
Copper block width	60 mm
Copper block height	40 mm
Coolant passage diameter	12 mm
Continuous water flow rate	6 l/min
Incoming water temperature	4 °C
Distance from weld	12 mm

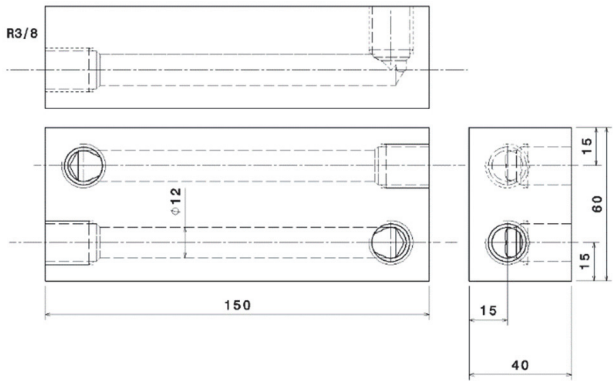

Fig. 13. Cooling block technical drawing (mm) (Reprinted under CC BY 4.0 license from Paper III © 2019 Authors).

The temperature of the weld was measured at two separate locations: the middle of the weld length-wise and 20 mm from the end point of the weld. The thermocouple wires can be seen in Fig. 11. The temperature range that was studied was between 800 and 100 °C. The thermocouple type used in the experiments was K20-2-350, which has a maximum temperature limit of 1200 °C. The thermocouple measures the temperature from the closest short-circuit point, which in this experiment was the lower surface of the weld root. The frequency used in the temperature measurement was 30 Hz. Three weld runs were done with and without the cooling blocks with constant welding parameters and the same welding robot program.

3.3 Welding experiments 960 MC

The welding experiments for commercial grade steel 960 MC were done with the same equipment that was used in the cooling potential experiment. In this experiment the temperature was measured only from the middle of the weld. The welding setup with the thermocouple wires in it can be seen in Fig. 14 and the joint geometry in Fig. 15. In this experiment, two weld passes were used to weld 8 mm thick 960 MC steel that had a minimum yield strength ($R_{p0.2}$) of 960 MPa and a minimum impact strength of 27 Joules at -40 °C and its alloying element content can be seen in Table 9 [53,Paper IV].

Table 9. Chemical composition of 960 MC (wt.% max) [53] (Reprinted under CC BY 4.0 license from Paper IV © 2019 Authors).

C	Si	Mn	P	S	Cr	Al (min %)	Nb	V	Ti
0.12	0.25	1.30	0.020	0.010	0.80	0.015	0.05	0.05	0.07

The steel has the carbon equivalent (CEV) of 0.51 in the case of 960 MC, which means that welding the steel is challenging [53]. The recommended $t_{8/5}$ for the steel is between 5 and 15 seconds, according to the manufacturer [52], meaning that the $t_{8/5}$ of the steel must be controlled strictly if a matching weld is desired. The welding parameters that were used are shown in Table 10 [Paper IV].

Table 10. Welding parameters used in the experiment (Reprinted [adapted] under CC BY 4.0 license from Paper IV © 2019 Authors).

Parameter	Value
Current	240 A
Voltage	22.9 V
Travel speed weld pass one	600 mm/min
Travel speed weld pass two	400 mm/min
Angle of the weld torch	17°
Welding technique	Push
Wire feed	6.2 m/min (Aristorod 89, Ø1.2 mm)
Welding energy weld pass one	0.55 kJ/mm
Heat input weld pass one	0.44 kJ/mm
Welding energy weld pass two	0.82 kJ/mm
Heat input weld pass two	0.66 kJ/mm
Gas flow rate	18 l/min (Mison 25)

The joint geometry can be seen in Fig. 15 and the welding setup in Fig. 14. The steel plates had a thickness of 8 mm, a width of 120 mm, and the length of the weld was 145 mm. The cooling curve of the welds was measured by using the same type of thermocouple as was used in the cooling potential welding experiment. However, in this experiment the temperature was measured only from the middle of the weld [Paper IV].

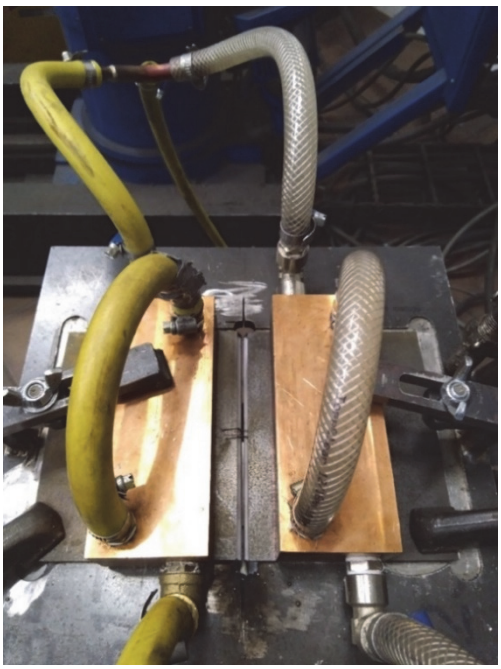

Fig. 14. The welding setup with thermoelement and cooling blocks (Reprinted under CC BY 4.0 license from Paper IV © 2019 Authors).

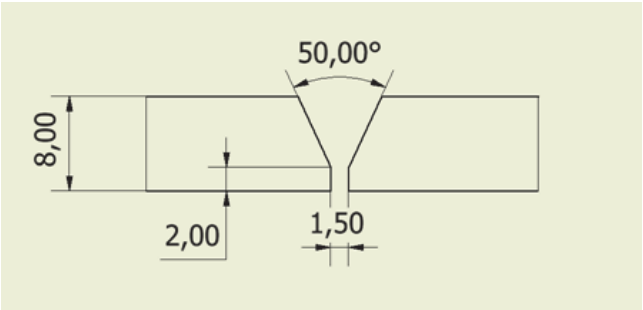

Fig. 15. Joint dimensions (Reprinted under CC BY 4.0 license from Paper IV © 2019 Authors).

Two different kinds of specimens were prepared from the welded joint: Charpy-V and flat tensile strength specimens. The Charpy-V specimens had the same dimensions as in the Gleeble experiments for 700 MC and 960 QL steels—5x10x55 mm—and the impact toughness testing was done at -40 °C according to

ISO 148-1. The flat tensile strength specimens had a width of 12 mm in the 75 mm long reduced section with the weld at its middle. The gauge length used was 50 mm and the specimens were taken from the middle of the plates thickness-wise by milling 2.5 mm off from both sides of the plate. The experiments were done with a Zwick 100kN testing machine [Paper IV].

3.4 Gleeble experiments for 960 MC ICCGHAZ

The Gleeble experiments were done in order to provide homogeneous ICCGHAZ for the impact toughness tests as well as to provide homogeneous ICCGHAZ specimens with which the microstructural differences could be studied by using high-resolution secondary electron imaging (SEI) in a field emission scanning electron microscope (FESEM). Furthermore, by using Gleeble, the welding defects and scatter caused by a heterogeneous weld can be avoided [Paper IV].

The Gleeble experiments were done as double-cycle simulations with peak temperatures of 1350 and 750 ℃ according to the cooling rate data that was measured during the welding experiment. The heating rate used was 400 °C/s and the soaking time was one second at peak temperatures. The cooling rates that were measured can be seen in Tables 11 and 12 [Paper IV].

Table 11. Cooling times for first Gleeble run (Reprinted under CC BY 4.0 license from Paper IV © 2019 Authors).

Temperature (°C)	Cooled, pass 1 (s)	Normal, pass 1 (s)
1350	0	0
800	2.8	2.8
700	3.8	3.8
600	4.8	5.1
500	7	7.3
450	9.5	10.5
400	12	13.1
350	16	17.1
300	20.6	22.6
250	27.4	30.8
200	38.6	43.4
150	58.6	67
100	93.8	118.6

Table 12. Cooling times for second Gleeble run (Reprinted under CC BY 4.0 license from Paper IV © 2019 Authors).

Temperature (°C)	Cooled, pass 2 (s)	Normal, pass 2 (s)
750	0	0
600	5	5.2
500	11	11.2
450	16.6	17.6
400	23.4	24.4
350	31.8	32.8
300	42.2	44.6
250	55.8	61.6
200	74.6	87.6
150	104.2	133.2
100	152.6	230

3.5 Improved heat sinks and their effect on mechanical properties and cooling time of single-pass welded 700 MC Plus

The welding equipment used in this experiment was the same as in the previous ones, excluding the welding jig that was designed to have less of an effect on the cooling of the weld, the welding wire, and the cooling blocks. The cooling blocks used in this experiment also had a new design to improve the approachability and

for them to be able to be used for longer weld seams. The new cooling blocks can be seen in Fig. 16 [Paper V].

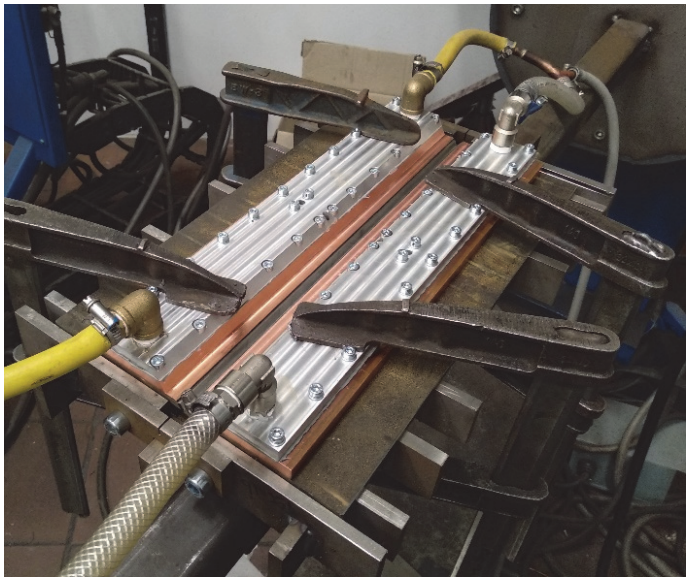

Fig. 16. Heat sinks on the steel plates (Reprinted under CC BY 4.0 license from Paper V © 2020 Authors).

The length of the weld seam was 400 mm and the dimensions of the plates being welded were 400x120x6 mm. The joint type was a V-groove butt-weld joint with a groove angle of 50 degrees. The steel that was welded was commercial grade steel with a minimum specified yield strength ($R_{p0.2}$) of 700 MPa, tensile strength (R_m) in the range of 750–950 MPa, an elongation to fracture (A_5) of at least 13%, and a specified minimum impact strength of 40 Joules at -60 °C in the longitudinal direction. The alloying elements used and their amounts can be seen in Table 13. Based on the manufacturer's recommendations the $t_{8/5}$ time for the steel is between 1 and 20 seconds with a maximum interpass temperature of 100 °C and a maximum heat input of 0.9 kJ/mm [54,Paper V].

Table 13. Chemical composition of steel (wt.% max) [54] (Reprinted under CC BY 4.0 license from Paper V © 2020 Authors).

C	Si	Mn	P	S	Al (min %)	Nb	V	Ti
0.12	0.25	2.10	0.020	0.010	0.015	0.09	0.20	0.15

The heat input used in the experiment along with the other parameters can be seen in Table 14 and the cooling block dimensions are shown in Table 15. The temperature of the weld seam and the steel was measured with the same thermocouple type—K20-2-350—as in the previous experiments. The temperature was measured from three different locations. One thermocouple was attached to the weld seam itself at the middle of the weld. This thermocouple was connected to the weld about 35 seconds after the weld torch had turned off with an error margin of about 5 seconds. The second thermocouple was positioned about 85–90 mm from the middle of the weld seam and the third one 5–10 mm from the end of the plate. The locations of the thermocouples can be seen in Fig. 17 [Paper V].

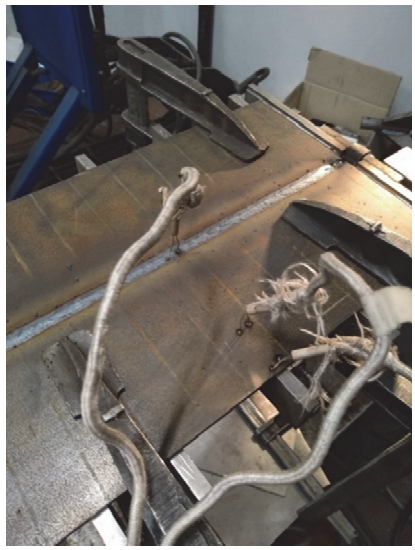

Fig. 17. Welded joint with all the thermocouples attached (Reprinted under CC BY 4.0 license from Paper V © 2020 Authors).

All of the specimens were taken transverse to the rolling direction. Furthermore, all of the specimens were taken between 50 and 350 mm length-wise to minimize cooling time differences, as the weld cools faster at the ends of the weld. All of the specimens were taken depth-wise from the middle of the weld by machining 1.5 mm from each side of the plate. In the case of both normal and cooled weld runs, three runs were used for each set. From each weld two tensile, two Charpy, and eight fatigue strength specimens were taken, but some specimens had to be eliminated due to surface defects [Paper V].

The Charpy V-notch specimens were water cut from the weld in longer sections than their final 5x10x55 mm dimensions, allowing for the correct positioning of the V-notch. The Charpy specimens were etched and then machined to their correct dimensions, leaving the V-notch in the fusion line. The total amount of specimens used in the impact toughness tests was five specimens per series. The specimens were machined following the same standard 100045-1 as in the previous experiments, and the ductile fracture percentage was evaluated following the same standard as before. The impact strength tests were conducted at -40 °C [Paper V].

The tensile strength specimens were 3 mm thick flat specimens that had the width of 12 mm and a 75 mm long reduced section. The weld was located at the middle of the reduced section length wise. The gauge length used in the tensile testing was 50 mm. Four specimens were used for both series [Paper V].

The fatigue strength samples underwent high-cycle life tests and followed ASTM E 466 standard [55], and the surface finishing of the specimens was done with sandpaper that had an ISO grit of P1200. The specimens were flat plate specimens that were 3 mm thick with a nominal width of 8 mm, a uniform length of 20 mm, radius R was 25 mm, and the total width of the specimens was 20 mm. As with the tensile specimens, the weld was located in the middle of the specimens. For fatigue strength tests, 17 normal specimens and 13 cooled specimens were used. Out of these specimens, three unbroken specimens that had reached 10 million cycles were reused for both series following the locati-method [56,Paper V].

Table 14. Welding parameters used in the experiment (Reprinted [adapted] under CC BY 4.0 license from Paper V © 2020 Authors).

Parameter	Value
Current	220 A
Voltage	22.2 V
Travel speed	320 mm/min
Angle of the weld torch	17°
Arc energy	0.92 kJ/mm
Heat input	0.73 kJ/mm
Gas flow rate	18 l/min (Mison 25)
Wire feed	6.0 m/min (Aristorod 69 Ø1.2 mm)
Preheating temperature	21 °C

Table 15. Cooling block parameters (Reprinted under CC BY 4.0 license from Paper V © 2020 Authors).

Parameter	Value
block length	400 mm
block width	80 mm
block height	40 mm
Water flow	6 l/min
Water temperature	4 °C
Distance from weld	1 mm

4 Results

4.1 700 MC and 960 QL CGHAZ

4.1.1 Tensile properties and elongation

700 MC

When the CGHAZ of the 700 MC steel was cooled down rapidly, the tensile strength had an upward trend as the finish temperature to which the steel was cooled was lowered. This can be seen in Fig. 18. As for the yield strength, the trend was similar to the tensile strength with the faster cooling rate of 50 °C/s, but the changes in yield strength were not statistically significant with a confidence level of 95% for either cooling rate, unlike with tensile strength. Regardless of the trend that can be seen in Fig. 19 with the faster cooling rate, the differences between the forced cooling finish temperatures of 500 and 100 °C were insignificant regardless of the cooling rate [Paper I].

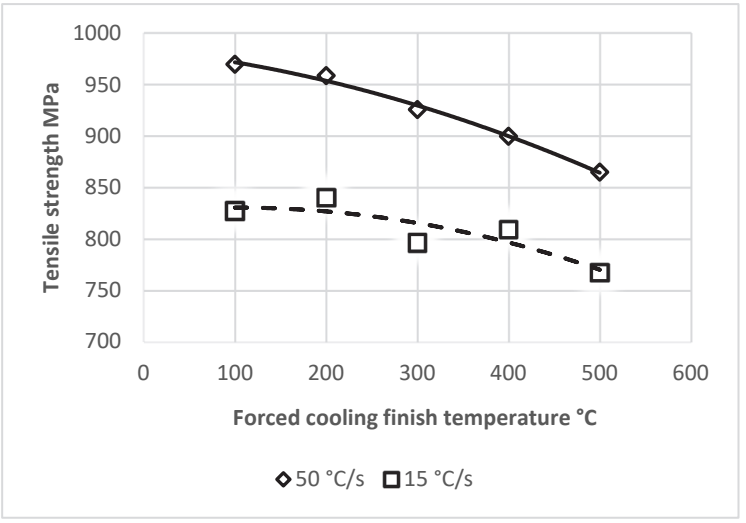

Fig. 18. Tensile strength of the CGHAZ for different cooling rates (700 MC) (Reprinted, with permission, from Paper I © 2017 International Institute of Welding).

The increase in tensile strength was 12% with the faster cooling rate of 50 °C/s and 8% with the slower cooling rate of 15 °C /s between 500 and 100 °C [Paper I].

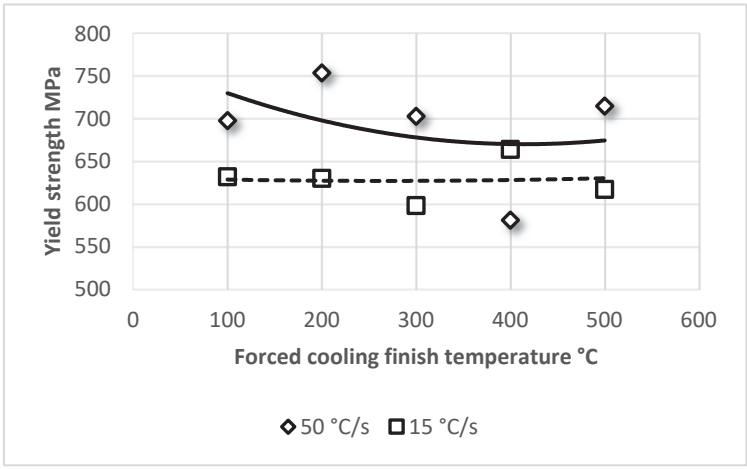

Fig. 19. Yield strength (0.2% proof stress) of the CGHAZ for different cooling rates (700 MC) (Reprinted, with permission, from Paper I © 2017 International Institute of Welding).

The increased tensile strength with both cooling rates caused the Y/T-ratio to improve as shown in Fig. 20 due to the yield strength remaining relatively unchanged. The lower Y/T-ratio is very beneficial to the steel because it gives the steel a higher tolerance against plastic deformation, which is very helpful when the steel is under a dynamic load [Paper I].

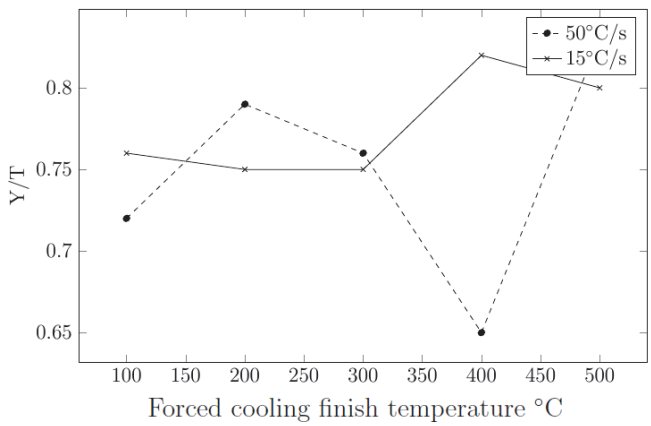

Fig. 20. Y/T ratios of the CGHAZ for different cooling rates (700 MC) (Reprinted, with permission, from Paper I © 2017 International Institute of Welding).

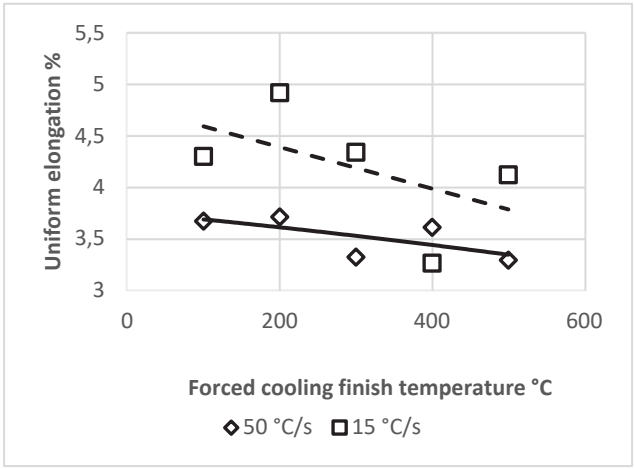

Fig. 21. Uniform elongation of CGHAZ for different cooling rates (700 MC) (Reprinted, with permission, from Paper I © 2017 International Institute of Welding).

As can be seen in Fig. 21, the lower forced cooling finish temperature had a similar effect as the tensile strength on the elongation of the steel. With a cooling rate of 50 °C/s, the elongation increased by 11.6% and by 4.4% with a cooling rate of 15 °C/s between the lower limits of 500 and 100 °C. Meaning that overall, from the point of view of strength and elongation, it would be very beneficial to the CGHAZ of 700 MC to rapidly cool the steel directly to the interpass temperature of 100 °C.

This would lead not only to time savings by eliminating a significant portion of the waiting time but also to improved tensile strength along with improved elongation [Paper I].

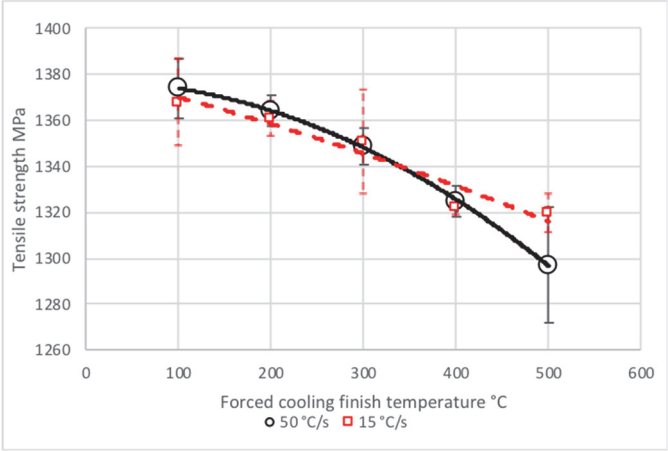

Fig. 22. Tensile strength of the CGHAZ (960 QL) (Reprinted, with permission, from Paper II © 2018 International Institute of Welding).

In the case of 960 QL, the tensile strength of the CGHAZ increased with both cooling rates as can be seen in Fig. 22. The effect of the cooling on the tensile strength was statistically significant (p-value of < 0.005). Furthermore, the tensile strength increased incrementally as the forced cooling finish temperature was lowered [Paper II].

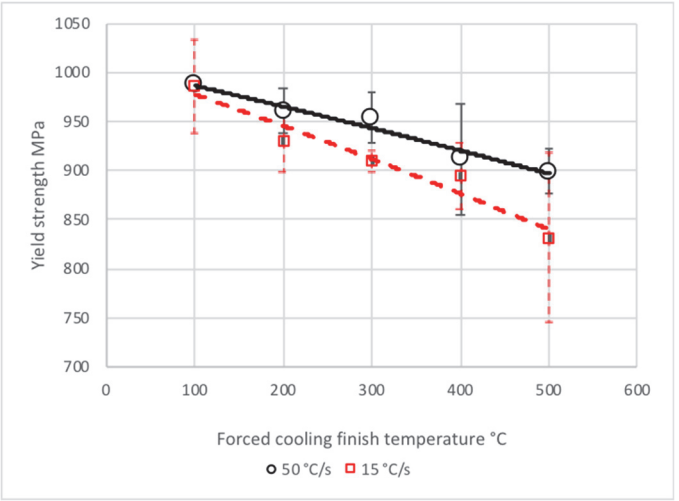

Fig. 23. Yield strength (0.2% proof stress) of the CGHAZ (960 QL) 15 °c/s P-0.036 (Reprinted, with permission, from Paper II © 2018 International Institute of Welding).

Unlike with 700 MC, the yield strength increases with 960 QL as the forced cooling finish temperature is lowered. However, only with the lower cooling rate is this change statistically significant with a p-value of 0.036. Nonetheless, it is likely that the yield strength increases with the faster cooling rate as well as due to the trend that can be observed in Fig. 23 [Paper II].

As both tensile and yield strength increased in the case of 960 QL when the forced cooling finish temperature was lowered, the Y/T-ratio suffered a little, as can be seen in Fig. 24. However, the increase in Y/T-ratio is still fully acceptable for most of structural applications due to the limit of an acceptable Y/T-ratio being 0.85 or below in most cases. Furthermore, the Y/T-ratio requirements are usually declared for the base material and not for the HAZ [57,58,Paper II].

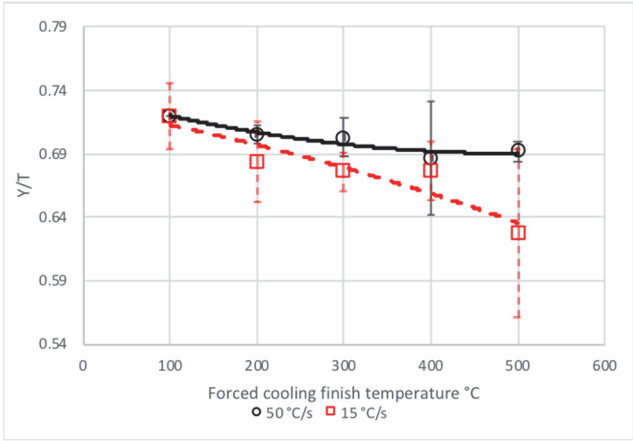

Fig. 24. Y/T ratios of the CGHAZ (960 QL) (Reprinted, with permission, from Paper II © 2018 International Institute of Welding).

From a statistical point of view, the forced cooling finish temperature did not have any effect on the elongation of the CGHAZ in this study. With the sample size of three for each parameter, the p-value was greater than 0.8 and no trend can be observed, as can be seen in Fig. 25 [Paper II].

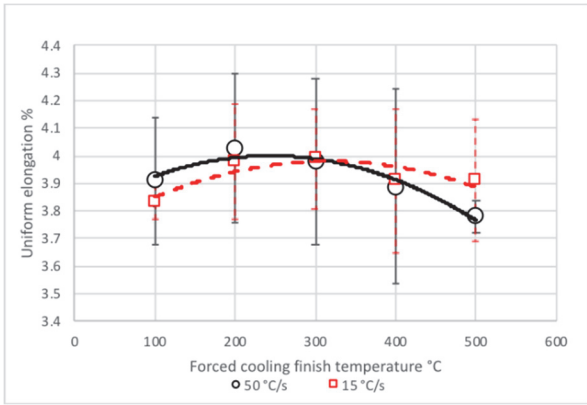

Fig. 25. Uniform elongation of CGHAZ (960 QL) (P>0.8) (Reprinted, with permission, from Paper II © 2018 International Institute of Welding).

4.1.2 Impact toughness

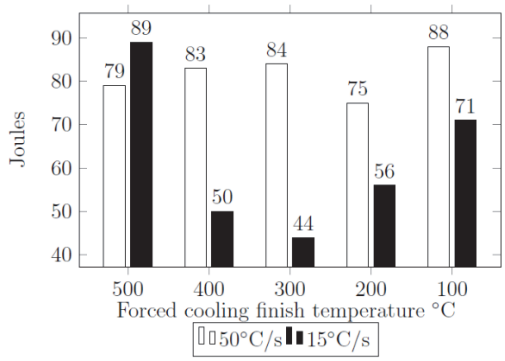

Fig. 26. Charpy V impact toughness at -40 °C for different cooling rates (700 MC) (Reprinted, with permission, from Paper I © 2017 International Institute of Welding).

Due to the significant scattering in the impact toughness tests, it cannot be claimed with certainty that the forced cooling finish temperature has any effect on the impact toughness of CGHAZ of 700 MC with the slower cooling rate of 15 °C/s. However, with the faster cooling rate of 50 °C/s there was less scatter and it could be that with a larger sample size the impact toughness of the CGHAZ does, in fact, improve when the steel is cooled rapidly to 100 °C. The mean impact toughness values can be seen in Fig. 26 and the individual impact toughness results and their respective ductile fracture percentages can be seen in Tables 16 and 17 [Paper I].

Table 16. Toughness values and percentage of ductile fracture at -40 °C for specimens cooled at 50 °C /s (700 MC) (Reprinted, with permission, from Paper I © 2017 International Institute of Welding).

FCFT, °C	#1	#2	#3	Median
500	76 J	78 J	83 J	78 J
	80%	*85%*	*100%*	85%
400	78 J	82 J	90 J	82 J
	100%	*100%*	*100%*	100%
300	70 J	90.5 J	92 J	90.5 J
	80%	*90%*	*100%*	90%
200	74 J	75 J	77.5 J	75 J
	70%	*75%*	*95%*	75%
100	82 J	82 J	99.5 J	82 J
	95%	*100%*	*100%*	100%

The ductile surface percentages did also improve with both cooling rates when cooled rapidly down to 100 °C, instead of cooling them rapidly to 500 °C. This further indicates that if the sample size was increased, there is a chance that the impact toughness could increase as well when the forced cooling finish temperature is lowered to 100 °C. In light of these results, it can at least be said with relative certainty that the impact toughness of the steel does not suffer when the forced cooling finish temperature is lowered to 100 °C [Paper I].

Table 17. Toughness values and percentage of ductile fracture at -40 °C for specimens cooled at 15 °C/s (700 MC) (Reprinted, with permission, from Paper I © 2017 International Institute of Welding).

FCFT, °C	#1	#2	#3	Median
500	73 J	92 J	102 J	92 J
	60%	*60%*	*70%*	60%
400	11.5 J	51 J	87 J	51 J
	20%	*40%*	*70%*	40%
300	15.5 J	50 J	68 J	50 J
	20%	*40%*	*50%*	40%
200	18 J	66 J	84 J	66 J
	20%	*50%*	*65%*	50%
100	14 J	92 J	107.5 J	92 J
	20%	*100%*	*100%*	100%

In the case of the impact toughness of 960 QL the cooling did not influence the impact toughness or the ductile fracture percentage if analyzed with a one-way ANOVA test with a p-value of 0.05. The mean values of the three samples for each parameter can be seen in Figs. 27 and 28 [Paper II].

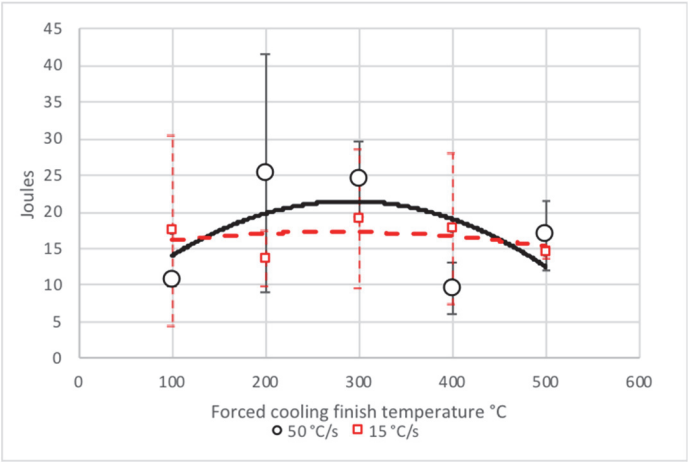

Fig. 27. Charpy V impact toughness at -40 °C (960 QL) with error bar of one standard deviation (Reprinted, with permission, from Paper II © 2018 International Institute of Welding).

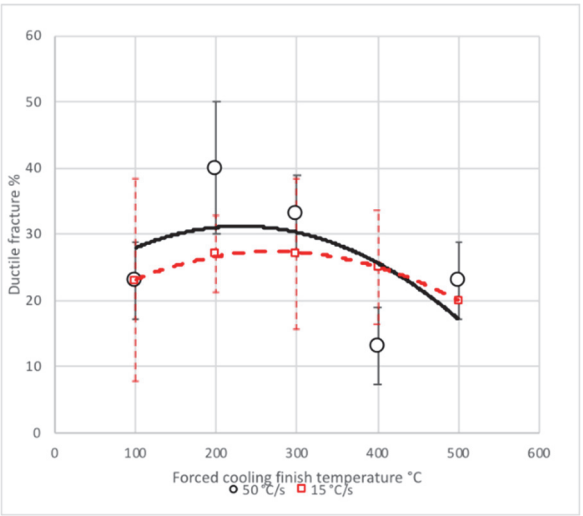

Fig. 28. Percentage of mean ductile fracture at -40 °C (960 QL) with error bar of one standard deviation (Reprinted, with permission, from Paper II © 2018 International Institute of Welding).

4.1.3 Microstructure

The differences that can be observed in the CHHAZ microstructure of the 700 MC are obvious, as can be seen in Fig. 29, when the steel is cooled down with the cooling rate of 50 °C/s and the differences between the forced cooling finish temperatures of 500 and 100 °C are compared. The CGHAZ that is rapidly cooled down to 100 °C displays a significantly larger quantity of lath-like structures that have finer lath thickness as well. This is likely to be caused by a larger quantity of lower bainite, because of the differences in mechanical properties and because of the refined carbide size and higher density of dislocations that are characteristic to lower bainite. The increased quantity of lower bainite would also explain the increase in tensile strength and elongation without having a negative effect on the impact toughness of the steel. Furthermore, it also indicates that there is the potential in some cases for the impact toughness to increase as well, because lower bainite has better impact toughness properties when compared to, for example, martensite [Paper I].

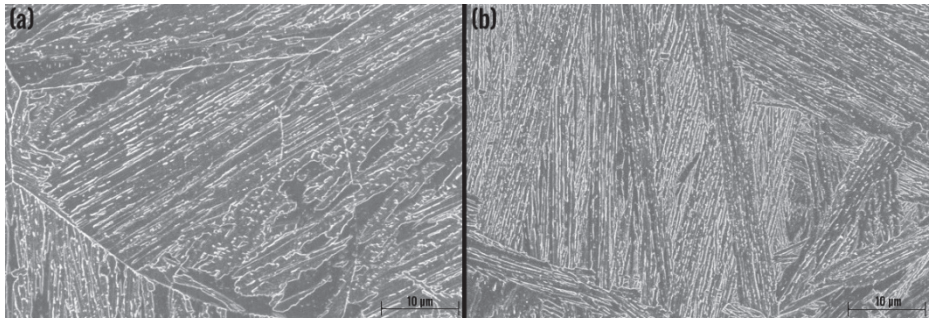

Fig. 29. Microstructure of the simulated CGHAZ with a cooling rate of 50 °C/s; (a) FCFT 500 °C, (b) FCFT 100 °C (700 MC, FESEM) (Reprinted, with permission, from Paper I © 2017 International Institute of Welding).

The microstructural differences in the CGHAZ of 960 QL can be seen in Fig. 30. As with 700 MC, microstructural changes are also evident in 960 QL when the forced cooling finish temperature is lowered. When the forced cooling finish temperatures of 500 and 100°C are compared, the quantity of martensitic laths is significantly greater with the FCFT of 100 °C. In addition to the increased quantity of martensite, the grain size is refined when the FCFT is lowered, which is highly beneficial to the impact toughness of the steel and counter-balances the potential negative effect an increased quantity of martensite has on impact toughness. The

combination of these two factors would also explain why impact toughness and elongation remained the same regardless of the FCFT, while the tensile and yield strengths of the steel increased [Paper II].

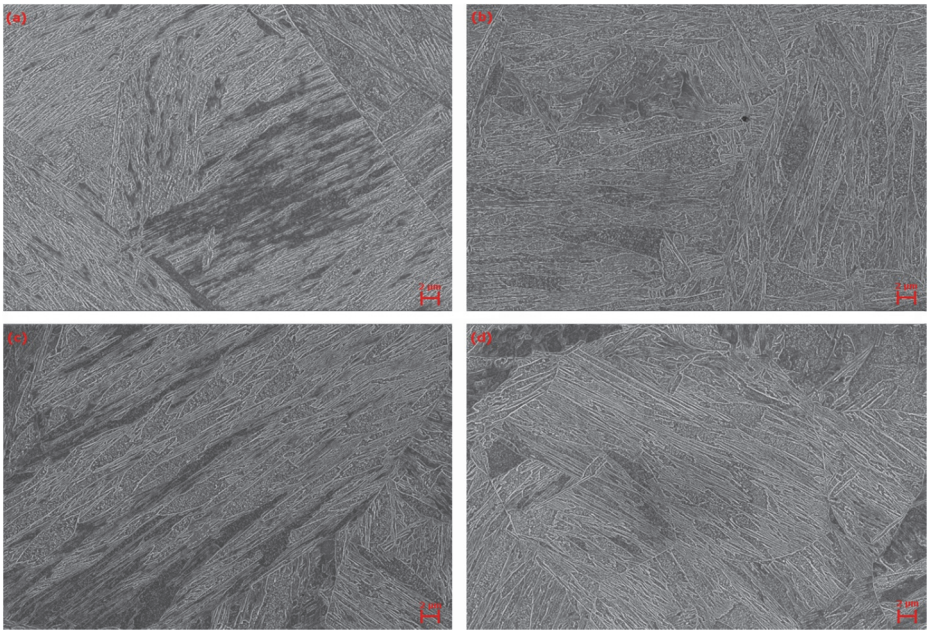

Fig. 30. Microstructure of the simulated h a cooling rate of 50 °C/s; (a) FCFT 500 °C, (b) FCFT 300 °C, (c) FCFT 200 °C, (d) FCFT 100 °CGHAZ (960 QL, FESEM) (Reprinted, with permission, from Paper II © 2018 International Institute of Welding).

4.2 Cooling time for 6 mm plate V-joint

The effect of the external cooling provided by the heat sinks was non-existent in temperatures above 550 °C as demonstrated in Fig. 31. Even at temperatures above 500 °C, the differences are relatively insignificant as can be seen from the $t_{8/5}$ time differences that are shown in Fig. 32. The differences in cooling curves start being significant below 300 °C when measured at the end of the weld and below 200 °C when measured at the middle of the weld [Paper III].

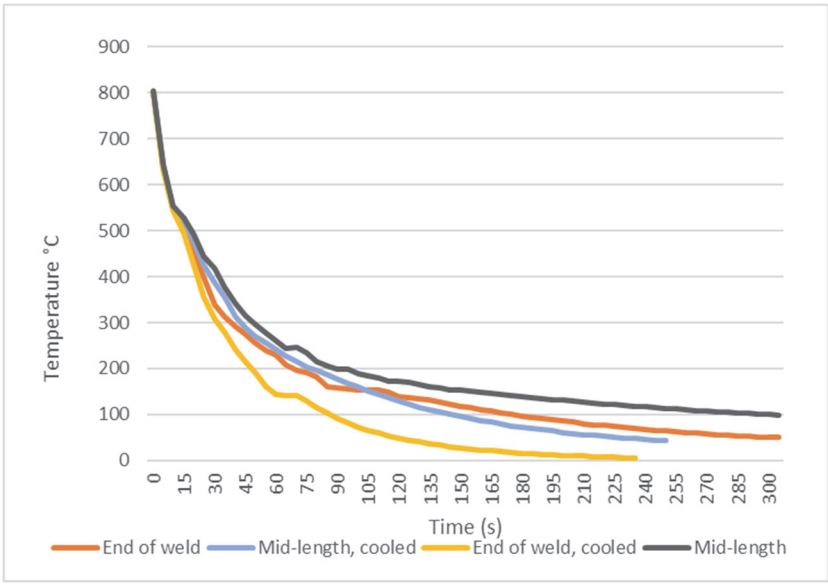

Fig. 31. The cooling curves of a single experiment (Reprinted under CC BY 4.0 license from Paper III © 2019 Authors).

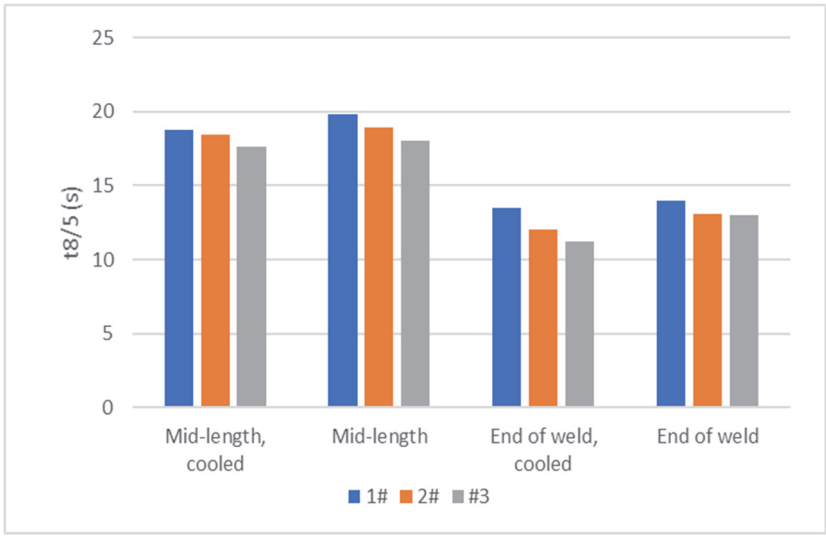

Fig. 32. Individual $t_{8/5}$ times for all of the experiments (Reprinted under CC BY 4.0 license from Paper III © 2019 Authors).

As the cooling curves do not deviate from each other significantly in temperatures above 500 °C, the $t_{8/5}$ time differences between cooled and normal welds were nonexistent as can be seen in Fig. 32. However, in the case of $t_{8/1}$, which is important from a multipass welding point of view, the differences in the cooling times were very significant as can be observed in Fig. 33 [Paper III].

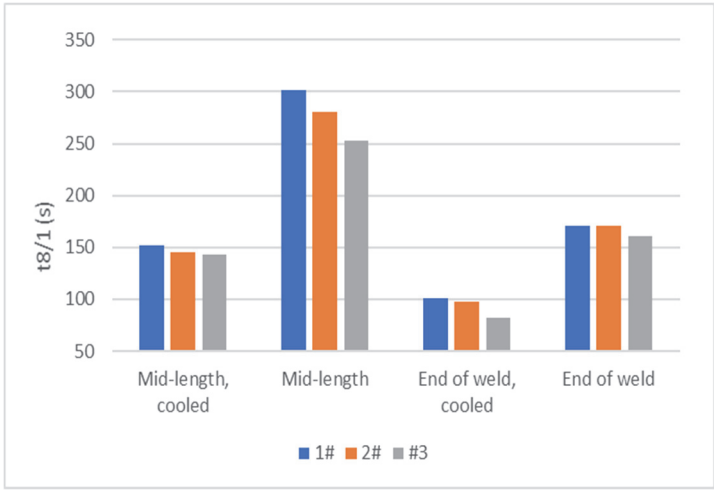

Fig. 33. Individual $t_{8/1}$ times for all of the experiments (Reprinted under CC BY 4.0 license from Paper III © 2019 Authors).

On average the $t_{8/1}$ was shortened by 132 seconds at the middle of the weld and by 74 seconds at the end of the weld when cooling was applied. This means that the cooling time can be reduced by up to 44–47%. This could translate to significant time savings in multipass welding processes if external cooling could be applied to shorten the time between weld passes, as the interpass temperature is often 100 °C [Paper III].

4.3 960 MC welding experiment and ICCGHAZ

4.3.1 Cooling time results

In the case of multipass welded steel with a plate thickness of 8 mm, the difference in cooling times to 100 °C was slightly less than in the previous experiment with a 6 mm thick single-pass welded plate. As can be seen in Figs. 34 and 35, the external

cooling does not really have any significant effect on cooling rates in temperatures above 500 °C [Paper IV].

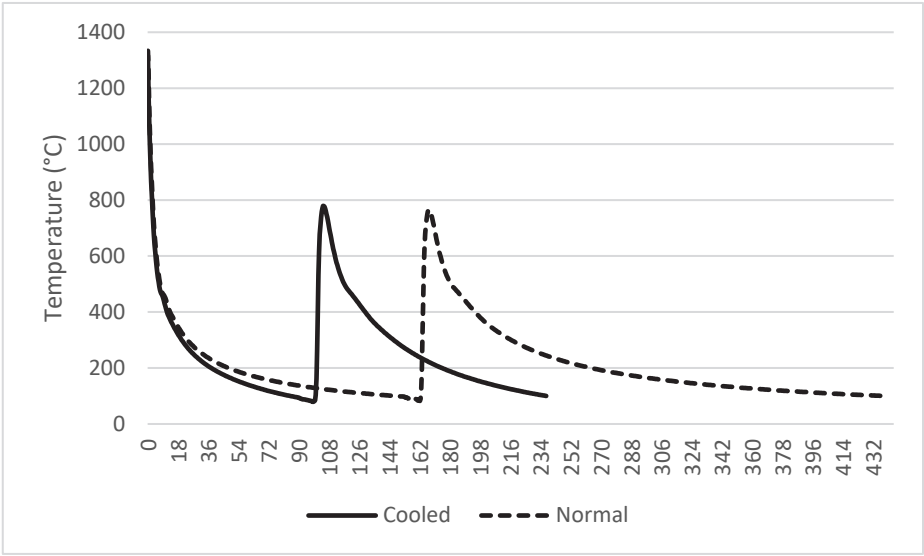

Fig. 34. Cooling curves of the weld (Reprinted under CC BY 4.0 license from Paper IV © 2019 Authors).

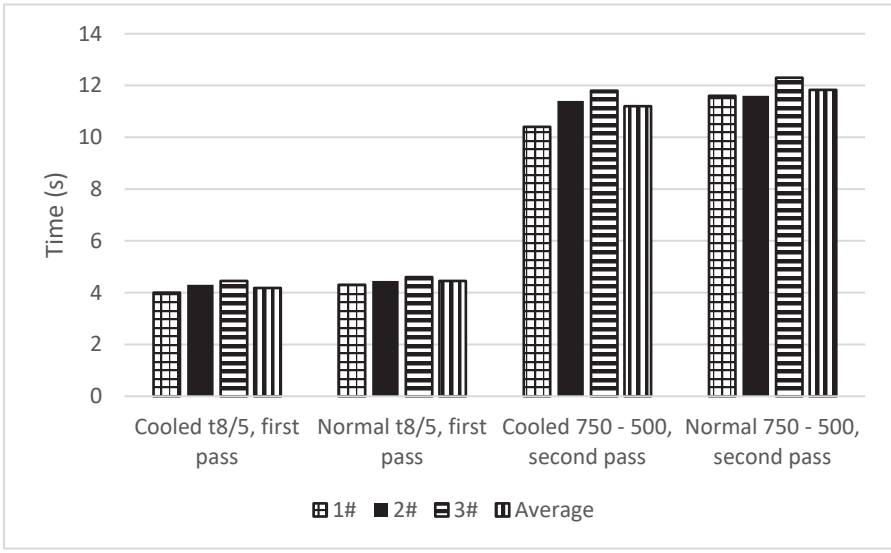

Fig. 35. Cooling times down to 500 °C (Reprinted under CC BY 4.0 license from Paper IV © 2019 Authors).

In temperatures below 300 °C, the cooling rates begin to differentiate from each other significantly which leads to large differences in the $t_{5/1}$ cooling time as can be seen in Fig. 36. The average time savings in $t_{8/5}$, $t_{5/1}$ and total time saved on average can be seen in Table 18 [Paper IV].

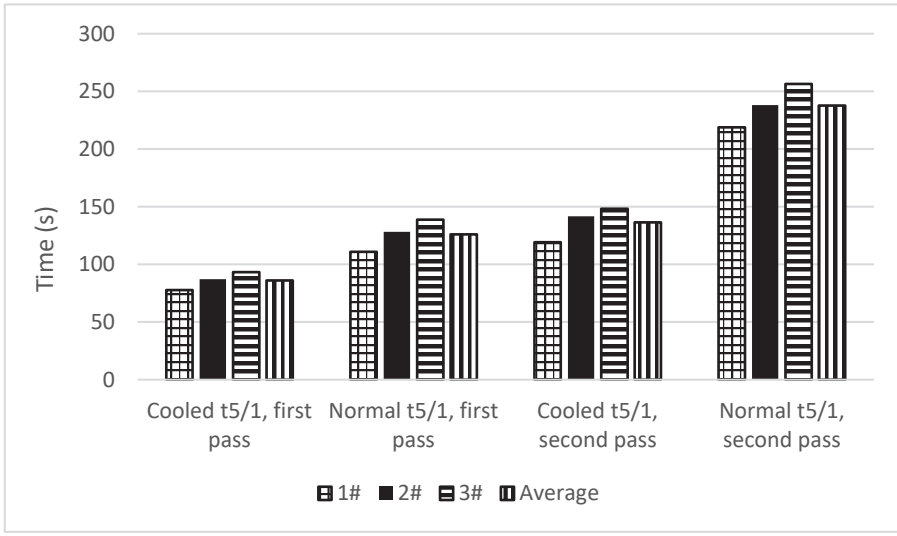

Fig. 36. Cooling times down to 100 °C (Reprinted under CC BY 4.0 license from Paper IV © 2019 Authors).

Table 18. Time saved by utilizing copper cooling blocks in the welding process (Reprinted [adapted] under CC BY 4.0 license from Paper IV © 2019 Authors).

Cooling phase	Time saved on average (s)
$t_{8/5}$, first pass	0.27
$t_{5/1}$, first pass	39.9
750–500, second pass	0.63
$t_{5/1}$, second pass	101.3
Total	142.1

The time that can be cut from the welding process can reach 33% if the second cooling cycle is included in the calculations, which could translate to significant time savings in the industry, if the time saved can be utilized in a productive manner [Paper IV].

4.3.2 Tensile properties and elongation of the welded joint

It is very likely that the tensile strength of the steel increases with external cooling, however, with the sample size of 3, the p-value was 0.069. This means that with the number of samples used, it cannot be guaranteed that the tensile strength increases with external cooling but it is likely that it does based on previous Gleeble

tests. One reason why the tensile strength might not have increased as clearly in this case was the lower cooling rate when compared to the Gleeble tests. The tensile strength grew on average by 4.2%. In the case of yield strength, the p-value was 0.00018 and the average yield strength grew by 9.1%. The numerical values of average tensile and yield strengths can be seen in Fig. 37 [Paper IV].

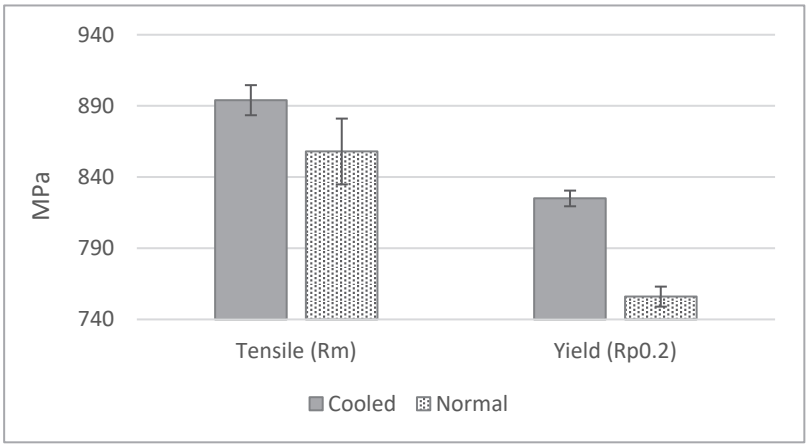

Fig. 37. Mean tensile and yield strengths with error bars indicating one standard deviation (means of 3 specimens) (Reprinted under CC BY 4.0 license from Paper IV © 2019 Authors).

As can be seen in Fig. 38, the uniform elongation decreased when cooling was applied. However, significant scatter was present, and the p-value was 0.818, which means that it cannot be said with certainty that the elongation decreases or increases. Although the scale of the results does demonstrate that the differences in uniform elongation are not very significant in any case. The Y/T-ratio, however, is in line with the elongation result. The Y/T ratio increased with the enhanced cooling by about 0.04 points, which is shown in Fig. 39. As the Y/T-ratio was already over 0.8, it is unlikely that the welded joint should be exposed to dynamic loading as it is. However, the 0.04 point difference has to be taken into account if the joint is exposed to dynamic stress [Paper IV].

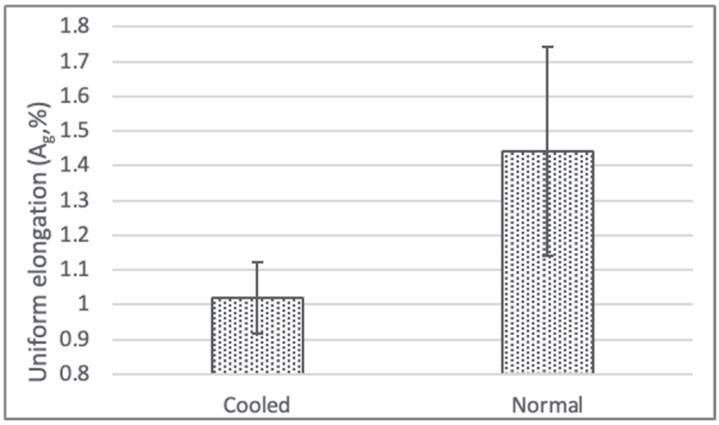

Fig. 38. Percent uniform elongation with error bars indicating one standard deviation (means of 3 specimens) (Reprinted [adapted] under CC BY 4.0 license from Paper IV © 2019 Authors).

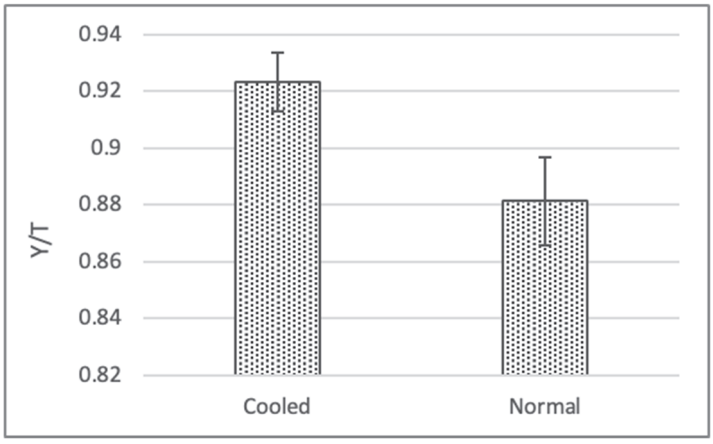

Fig. 39. Y/T-ratio with error bars indicating one standard deviation (means of 3 specimens) (Reprinted [adapted] under CC BY 4.0 license from Paper IV © 2019 Authors).

4.3.3 Impact toughness of the joint and Gleeble simulated ICCGHAZ

In the case of ICCGHAZ Gleeble simulated welds as well as fusion line specimens taken from the weld itself, the impact toughness clearly improved with the

enhanced cooling, as shown in Fig. 40. The impact toughness results were statistically significant as well with the p-value being less than 0.03 in both comparisons. On average the impact toughness increased by 8.4 Joules with the ICCGHAZ Gleeble samples and by 7.5 Joules in the case of fusion line samples. These results translate to 25% and 18% impact toughness improvements.

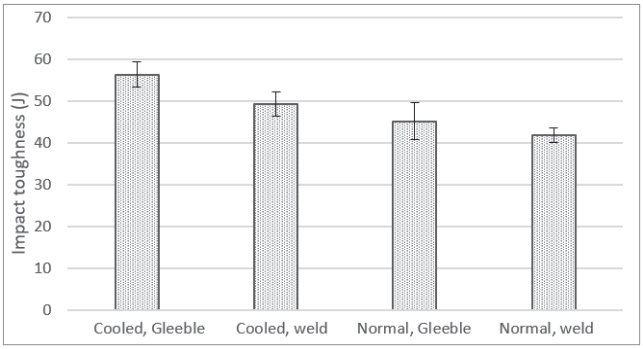

Fig. 40. Mean impact toughness at -40 °C with error bars indicating one standard deviation (means of 3 specimens) (Reprinted under CC BY 4.0 license from Paper IV © 2019 Authors).

The fracture surface percentage increased as well when enhanced cooling was applied as shown in Fig. 41. This result is in line with the impact toughness results, as it is logical that a larger ductile fracture percentage leads to higher impact toughness results. The ductile fracture surface results were statistically significant as well with the p-value being under 0.05. The ICCGHAZ samples had no scatter at all in the ductile fracture percentages, but the normal welds did, as can be expected since real weld joins are not as homogeneous as simulated ones [Paper IV].

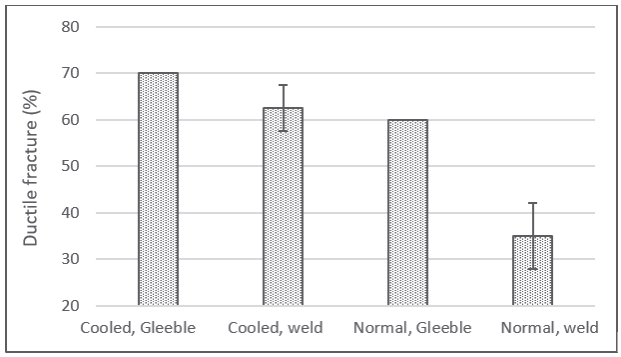

Fig. 41. Mean percentage ductile fracture with error bars indicating one standard deviation (means of 3 specimens; the Gleeble samples showed no scatter at all) (Reprinted under CC BY 4.0 license from Paper IV © 2019 Authors).

4.3.4 ICCGHAZ microstructure

The enhanced cooling did not have a significant effect on the grain size of the ICCGHAZ when the grain size was calculated by using the areas seen in Fig. 42. The mean linear intercept grain size decreased from 48 to 46 µm when the specimen was cooled. However, there was lot of scatter in the grain sizes so the result is not significant [Paper IV].

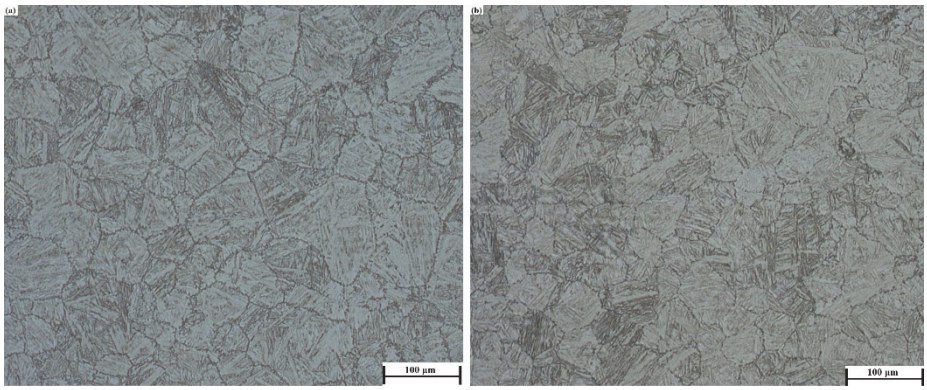

Fig. 42. Microstructural image of (a) cooled and (b) normal simulated ICCGHAZ specimens. FESEM SEI with 5x magnification (Reprinted under CC BY 4.0 license from Paper IV © 2019 Authors).

The dominant microstructure remained the same regardless of the cooling rate, and both samples were mostly martensitic-bainitic. The cooling did, however, produce larger MA-constituents as can be seen in Fig. 43. In addition, the cooled samples had less carbides and they were finer than in the normal samples. MA-constituents usually cause the steel to become more brittle as they are necklaced and play a significant part in the propagation of cleavage crack nucleation [30,59]. However, the larger the carbides are, the more detrimental they are to the mechanical properties of the steel, and in this case the effect of rougher carbides seemed to negate the effect that the MA-constituents have on the joint [60,61,Paper IV].

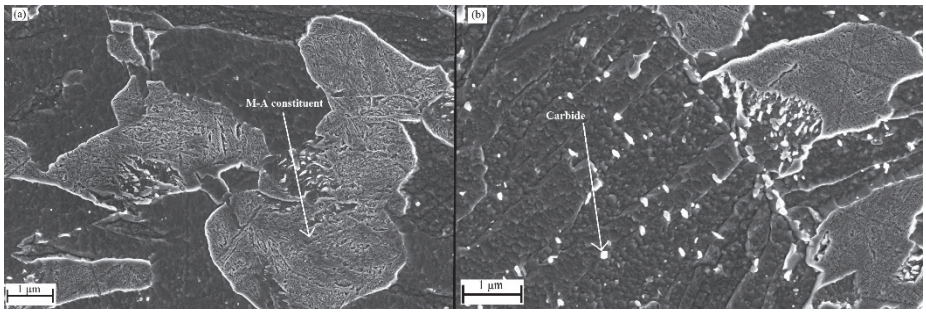

Fig. 43. Microstructural image of (a) cooled and (b) normal samples with 30x magnification (FESEM) (Reprinted under CC BY 4.0 license from Paper IV © 2019 Authors).

4.4 700 MC Plus with improved heat sink experiments

4.4.1 Cooling potential provided by the heat sinks

The cooling potential of the newly designed cooling blocks was significantly better than the previously used cooling blocks. The blocks cooled the weld down to temperatures around 90 °C by the time the thermocouple was attached to the weld. This means that the weld had cooled down to temperatures below 100 °C in less than 40 seconds given that it took around 35 seconds to attach the thermocouple with the error margin of 5 seconds. After the thermocouples were attached, the measured cooling rate between temperatures of 90–50 °C was 1.23 °C/s on average. The thermocouples attached to the plates being welded outside of the weld seam saw only a temperature increase of around 3–5 °C [Paper V].

Without the heat sinks the temperature of the weld was 230 °C by the time the thermocouples were successfully connected. The cooling rates that were measured at temperatures below 230 °C can be seen in Fig. 44. Furthermore, the time it took for the steel to cool down to 100 °C, which is the ideal interpass temperature for high-strength steels, was about 244 seconds. In addition to a significant cooling time difference between the cooled and non-cooled welds, the whole plates that were being welded experienced a clear rise in their temperature when the heat sinks were not used. The thermocouple that was attached near the edge of the plate experienced a maximum temperature of 68 °C and the thermocouple located 85 mm from the weld experienced a maximum temperature of 79 °C. Furthermore, the whole plate remained hot for several minutes and the thermocouples reached temperature equilibrium at around 50 °C [Paper V].

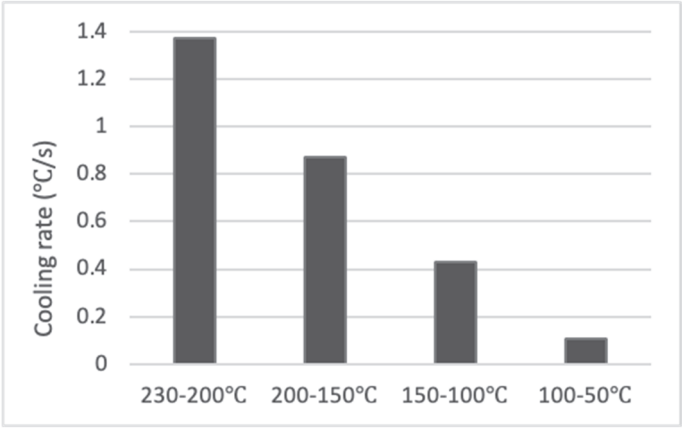

Fig. 44. Median cooling rates for welds without external cooling (Reprinted under CC BY 4.0 license from Paper V © 2020 Authors).

The difference between the cooling times it took for the weld to reach 100 °C was at least 200 seconds on average with the parameters used in this experiment. In multipass welding applications, introducing external cooling could be very useful as it would make the interpass temperature of 100 °C more viable from an economical point of view as the waiting time would be nearly eliminated. A lower interpass temperature would allow for higher heat input for the consecutive weld passes as well, and a higher heat input means that the consecutive weld passes would have a higher material deposition rate. This could translate to a smaller number of weld passes being required to fill the weld gap. From a quality point of

view, this would be very desirable as it would minimize the amount of LBZs in the joint [42,Paper V].

4.4.2 Impact toughness

In the case of 700 MC Plus, the external cooling did not have an effect on the impact toughness as the p-value was significantly higher than 0.05. Furthermore, one of the normal impact toughness specimens was excluded from the median values that are shown in Fig. 45, due to it being a clear outlier with an impact toughness value of 61 Joules. As the impact toughness tests were done at -40 °C, it is very likely that the transition temperature is around the testing temperature and caused the specimen to have a significantly higher value compared to the other specimens [Paper V].

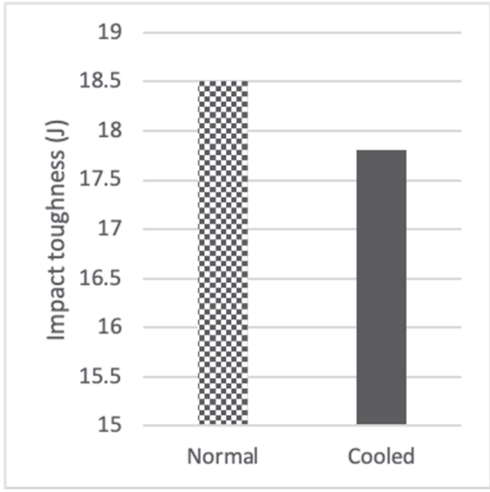

Fig. 45. Median impact toughness of 700 MC Plus (Reprinted under CC BY 4.0 license from Paper V © 2020 Authors).

The cooled specimens had an average ductile fracture percentage of 49% and the normal specimens 40%. The difference was not statistically significant with the 95% confidence interval. Therefore, it can be said that it is likely that the external cooling does not have an effect on the impact toughness of the steel used in this experiment in single-pass welding applications [Paper V].

4.4.3 Tensile properties

As with previous experiments, the enhanced cooling increased the tensile and yield strengths of the weld. The average tensile and yield strengths can be seen in Fig. 46. The increase in tensile strength achieved by using the cooling blocks was 38 MPa and the increase in yield strength was 31 MPa. This translates to a 5.1% increase in tensile and a 4.7% increase in yield strength. The uniform elongation was improved as well by introducing the enhanced cooling to the welding process as can be seen in Fig. 47. The result is very similar to what was achieved in the first Gleeble experiment, in which the uniform elongation improved while the tensile and yield strengths improved as well. The tensile and yield strength results alongside with the uniform elongation results were statistically significant with the confidence interval of 95% [Paper V].

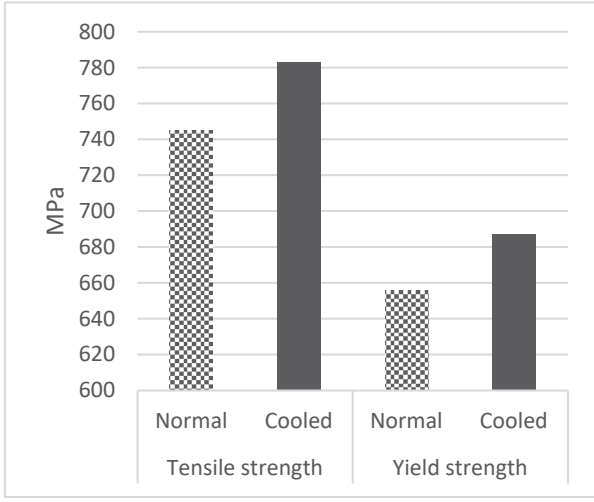

Fig. 46. Median tensile and yield strengths for 700 MC Plus (Reprinted under CC BY 4.0 license from Paper V © 2020 Authors).

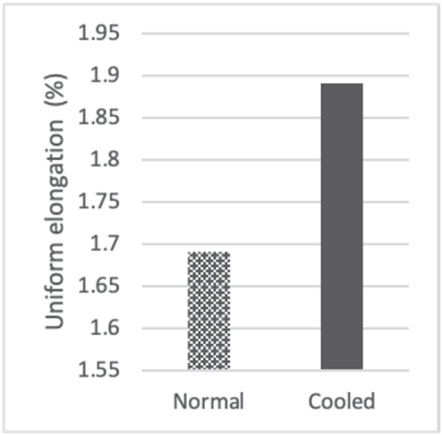

Fig. 47. Uniform elongation of 700 MC Plus (Reprinted under CC BY 4.0 license from Paper V © 2020 Authors).

Furthermore, all of the cooled specimens failed at the HAZ. In addition, all normal specimens, with the exception of one, broke at the HAZ as well. The one normal specimen that did not fail at the HAZ, failed at the fusion line instead [Paper V].

4.4.4 High cycle-life fatigue

The cooled specimens seemed to have a higher fatigue strength than the normal ones, as can be seen in Fig 48. All of the fatigue specimens failed at the fusion line. However, when the three specimens that had already undergone one fatigue experiment cycle without breaking until 10 million cycles were tested from each series, no significant difference was observed between the series. The experiment for these specimens followed the locati-method, in which the fatigue strength is raised in increments of 15 MPa until they break. As for the cooled specimens, they broke on average with the maximum stress of 650 MPa, and the normal specimens broke on average with the maximum stress of 645 MPa with the locati-method. Furthermore, the locati-method specimen results had no statistically significant differences between the two series [Paper V].

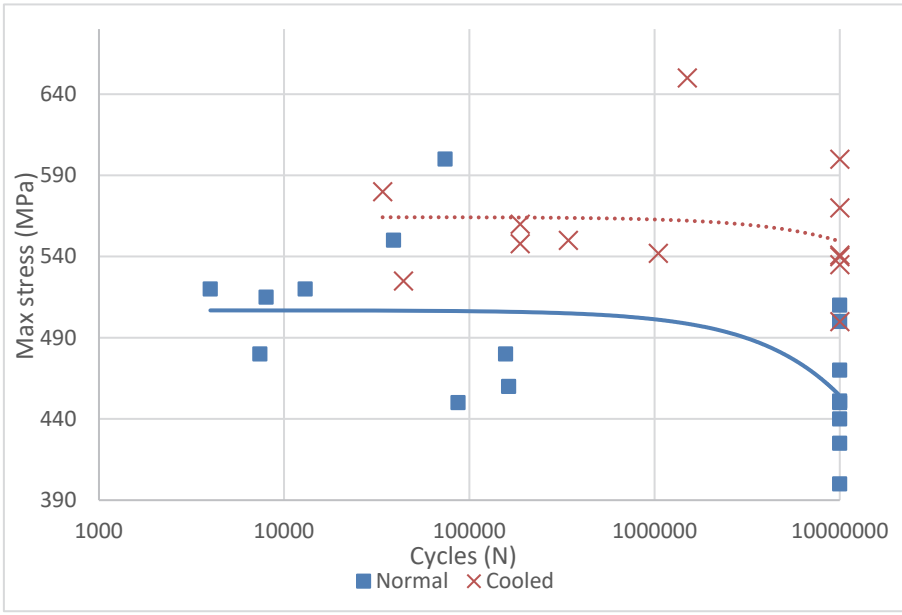

Fig. 48. Fatigue results for both normal and cooled welds (Reprinted under CC BY 4.0 license from Paper V © 2020 Authors).

As the residual stress difference disappeared during the first fatigue experiment run, it is likely that the difference in results, as seen in Fig. 48, is caused by the residual stress differences as there was no statistically significant difference between the two series in the locati-method experiment. It is known that external cooling can reduce the residual stresses in the welded joint. An experiment conducted by Jiang et al., demonstrated that external cooling that was placed under the material being welded reduced the residual stresses by 20% [44]. It is also known that residual stress has a significant effect on the fatigue strength of the steel [Paper V].

4.4.5 Microstructure

As can be seen in Fig. 49, the difference between the fusion lines of a cooled weld and normal one is striking. The external cooling clearly provides a different kind of fusion line, as the fusion between the weld metal and base material is more continuous over the normal weld, in which the fusion line between weld metal and base material is clear. This also means that the cooling rate provided by the cooling blocks had to be enhanced in temperatures above 500 °C as the solidification takes

place in temperatures above 500 °C. This is a clear improvement over the previously used cooling blocks that did not have a significant effect on the cooling rate of the steel in temperatures above 500 °C [Paper V].

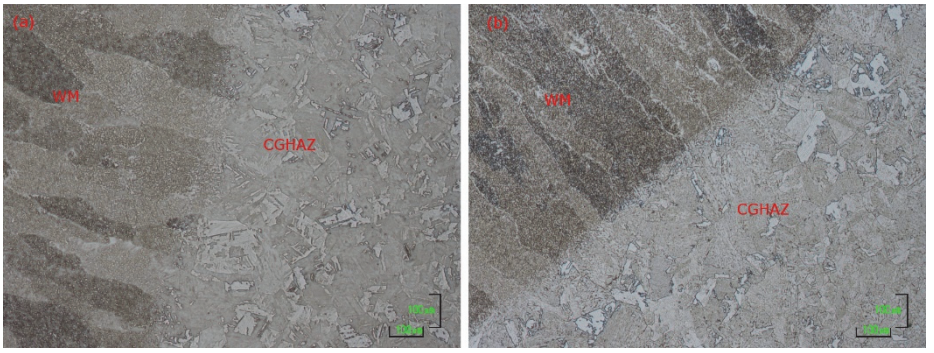

Fig. 49. Fusion line images (a) cooled, (b) normal (Reprinted under CC BY 4.0 license from Paper V © 2020 Authors).

The cooling provided by the blocks also provided a refined grain size in the CGHAZ, when calculated from the area seen in Fig. 50 with a linear intercept method. The grain size was reduced from 56.8 µm to 50.7 µm. Furthermore, the CGHAZ seems to demonstrate a more lath-like structure when it is cooled, and it is likely that the quantity of lower bainite has increased. If the quantity of martensite had increased, the uniform elongation would not have increased. In addition to the improved elongation, the tensile and yield strengths increased without any negative effect on the impact toughness, which could be explained by a larger quantity of martensite or bainite or by the finer grain size. However, martensite usually has a negative effect on impact toughness. Therefore, it could be that the factor that is behind the improved mechanical properties is a larger quantity of lower bainite that can be achieved with enhanced cooling rates. However, the possibility of increased quantity of martensite cannot be ruled out with certainty, as the steel did cool down very rapidly and low carbon martensite does not necessarily have a negative impact on impact toughness [Paper V].

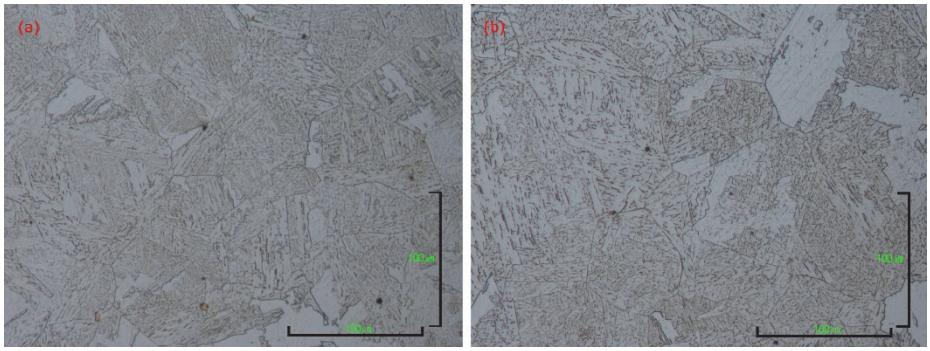

Fig. 50. CGHAZ images of the specimens (a) cooled, (b) normal (Reprinted under CC BY 4.0 license from Paper V © 2020 Authors).

5 Discussion and summary of results

It is clear that cooling the weld to sub-500 °C temperatures has an effect on the mechanical properties of the steel when the steel being welded is an ultrahigh- or high-strength steel with low amounts of alloying elements. With the steels that were used in the experiments, it was found that enhanced cooling had a positive or neutral effect when it was used to reach the often recommended interpass temperature of 100 °C. Excluding Y/T-ratios that did suffer slightly with 960 MC and 960 QL, because the tensile strength increased more than yield strength when cooled rapidly. This means that in some cases it might be worthwhile to introduce $t_{8/1}$ to replace $t_{8/5}$ if the best possible mechanical properties, such as yield and tensile strengths, are desired. This is because the enhanced cooling down to 100 °C proved to be a superior option over focusing only on the time it takes for the weld to cool down to 500 °C.

In the first experiment with Gleeble that utilized a commercial 700 MC steel and the last experiment in which other commercial 700 MC Plus steel was welded, an interesting phenomenon was observed. The tensile strengths increased while elongation increased as well when enhanced cooling was applied down to 100 °C. In most cases, elongation would decrease as tensile strength increases. Based on the microstructural images taken, it looks like lower bainite had formed in the CGHAZ of the steel, which would explain the increased strength and elongation without having negative effect on the impact toughness. Furthermore, the yield strength also increased in the welded specimens while it remained relatively unchanged in the Gleeble samples. Another interesting phenomenon observed was that the external cooling had an effect on the fusion line. The cooling caused the fusion line to be less distinct in the steel, meaning that the cooling had an effect on the solidification of the weld metal. Furthermore, in the same experiment the fatigue strength of the steel increased. The crack propagation of the fatigue strength specimens started in the fusion line in both the cooled and normal welds. External cooling reduces the residual stress and it has a positive effect on the fatigue strength. It does seem that the effect that the cooling has on the solidification and fusion line might have a positive effect on fatigue strength as well.

The 960 QL steel that was used in the Gleeble experiments also demonstrated increased tensile and yield strengths when it was rapidly cooled down to 100 °C instead of being cooled down to only 500 °C and then left to cool down to room temperature on its own. Cooling has no significant effect on the elongation or on the impact toughness of the CGHAZ. In the case of welding experiments done with

960 MC, the tensile and yield strength increased as well when enhanced cooling was used to reach 100 °C quicker, even though the tensile strength increase was not statistically significant with the confidence level of 95%. But given the previous Gleeble experiments it is likely that with a larger sample size the tensile strength would increase. Furthermore, it was observed that the impact toughness was improved by the external cooling. The following Gleeble experiments utilized cooling rates measured from the welds to produce simulated ICCGHAZ Charpy-V specimens. The impact toughness of the ICCGHAZ increased when the faster cooling rates were used to reach the same 100 °C. In the case of the welded specimens the uniform elongation did not change when external cooling was applied.

Therefore, the mechanical properties were either improved or remained unchanged in all of the experiments that were carried out on four different steels. This means that from a quality point of view, with these four steels, there is no reason why external cooling could not be introduced.

Furthermore, the characteristic features behind the improved mechanical properties were lower bainite and martensite formation, refined carbides, reduced grain size, and maybe the improved fusion between the weld metal and base material. The increased lower bainite formation was observed only with the steels with yield strength of 700 and the martensite formation in the steels with yield strength of 960 MPa. The enhanced cooling did reveal that it has the potential to produce negative microstructural changes as well. In the multipass welding experiment, the enhanced cooling caused MA-constitutes to be more prevalent and be necklaced. This is detrimental to the steel, but in this research the refined carbides counteracted this detrimental effect.

The enhanced cooling rates achievable with heat sinks that are placed on top of the plate and next to the weld proved to be significantly higher than without external cooling. When the cooling times between temperatures of 800 and 100 °C are compared, the possible time savings achievable varied between 40 and 200 seconds depending on the design of the heat sinks, heat input, thickness of the steel, and working temperature.

The improved heat sink design nearly doubles the amount of time saved as can be seen when the results of the first experiment and the last one are compared. In both experiments the working temperature and the thickness of the metal being welded were the same. Even though the latter experiment had a lower heat input by 0.1 kJ/mm, the time saved was significantly higher as can be seen in Table 19. However, as these were single-pass welding applications, the external cooling is

not as important from a productivity point of view. The most important information that can be derived from Table 19, is the improved cooling potential achievable with the improved heat sink design. The second and third rows in the table are the most notable ones as those are the results from the multipass welding experiment. If the ratio of improvement that can be achieved with the improved heat sink design holds true for multipass welding applications, for example, with an 8 mm thick steel, the time saved would exceed 50% and might even reach as high as 80%. Furthermore, in some situations multipass welding is used with 6 mm thick steels, which would translate to an even larger amount of time saved.

Table 19. Time saved by the heat sinks.

Heat input (kJ/mm)	Working temperature (°C)	Plate thickness (mm)	Time saved (s)	Time saved (%)	Heat sink design
0.83	21	6	94	45.5	Basic
0.44	21	8	40.17	30.8	Basic
0.66	100	8	101.93	40.8	Basic
0.73	21	6	200	83.6	Improved

As the waiting times can exceed 250 seconds per weld pass, the time savings that can be achieved by using the heat sinks have a clear impact on the production costs. Especially in production lines that have been optimized in a way where transportation, setting times, and other factors that cause time to be wasted have been minimized.

Factors such as the time that transporting the structure to and from the welding bench have to be taken into account, as well as the time it takes to attach the grounding cable to the steel and other factors that vary based on how the welding process is carried out. For example, in an automated welding line, the time saved by applying the heat sinks could be relatively close to the time saving percentages seen in Table 19, but in an optimized welding line that utilizes manual labor, the time saving that can be achieved would be significantly less. However, even in a manual setting, the total time saved by introducing the heat sinks to the process could be more than 10%.

Another way to improve efficiency when beam structures are being welded would be laser-based welding technologies, GMAW-P, or using other means of external cooling, such as liquid nitrogen, argon or solid carbon dioxide. However, the traditionally used cooling methods consume the medium they use and are

unfriendly to the environment and more costly to use when compared to the heat sinks that consume nothing. Furthermore, most of the welding in the world is still done by arc welding methods due to the high cost of acquiring laser-based welding equipment. Often modern brand-new high-performance laser welding systems cost over six figures. The laser-based welding technologies also require a joint with tighter tolerances, which means more pre-welding work. GMAW-P and other GMAW based welding ideas such as CMT are desirable options as they lower the heat input and the machines required are relatively cheap to acquire when compared to laser-based welding equipment. However, even with the various GMAW based techniques, multipass welding still is often required as the heat input caused by the welding process cannot be reduced enough to allow single-pass welding in all situations. This means that cooling is the way to enhance the productivity of the welding process without having to buy expensive equipment. Cooling can be used in tandem with the various welding techniques that have a lower heat input.

External cooling might also allow the use of higher heat input. If a higher heat input could be allowed, the number of required weld passes could be reduced, and in doing so the amount of LBZ's in the joint would be minimized. However, even if a higher heat input would not be allowed according to the previous point of view, the external cooling could make lower interpass temperatures more desirable for fabricators as the waiting times would be reduced. The lower the interpass temperature is, the higher the maximum allowable heat input is. Thus, the possibility of having the required amount of weld passes reduced is a very real factor in some situations. The reduced amount of weld passes would have a beneficial effect from a productivity point of view as it would eliminate some arc time as well.

Furthermore, the external cooling limits thermal expansion that takes place as a result of the base material significantly heating up. For example, the 6 mm thick steel experienced the maximum temperature of 79 °C when measured 85 mm from the weld and 68 °C when measured about 110 mm from the weld without external cooling. These measured temperatures reached equilibrium at 50 °C, which is still 29 °C higher than the ambient temperature and the original working temperature. Furthermore, this increase in temperature was caused by a single weld pass, meaning that with subsequent weld passes, the temperature would keep increasing. It is known that deformations caused by thermal expansion and compression as a result of welding can be problematic. Heat sinks could eliminate this almost completely as the steel only experienced a 3–4 °C increase in temperature when measured from the same points as in the case of the normal weld. Furthermore, the

slight increase in temperature was only present for less than a minute, meaning that subsequent weld passes would not have so high an impact on the working temperature with the heat sinks as they would without the heat sinks.

6 Conclusions and future

Cooling the weld directly to the common interpass temperature of 100 °C proved to be highly beneficial from the point of view of the mechanical properties and without any negative side effects. However, it remains unknown how much of an effect the cooling has on the ductile-to-brittle impact toughness transition temperature of the steel, as previous research conducted by Hoy et al. (2015) found that cooling the steel rapidly to low temperatures can have a negative effect on the transition temperature of the steel [62]. However, in this study the enhanced cooling provided by the heat sinks had a positive effect on the impact toughness values at -40 °C as well as on the weld as a whole and on the ICCGHAZ.

From a productivity point of view the heat sinks could shorten the production times by tens of percentages while reducing deformations that can be caused by the welding. Furthermore, the heat sink technology is more environmentally friendly than the alternatives, which consume the medium used to cool the weld. Heat sinks are also more efficient when compared to other cooling methods, such as liquid argon or compressed air. The heat sinks can be used with most structures as well, because they are placed next to the weld and on top of the steel instead of under the weld, which is practically impossible with beam structures.

However, further advanced research should be conducted concerning the effects of the cooling on the microstructure of individual steels and the causes behind improved tensile properties while elongation improves as well. In addition, fractography should be performed in cases in which the impact toughness improves to gain further information about the causes behind the changes in impact toughness. Furthermore, the effect of the heat sinks on the solidification and how it affects the fusion line should be researched in depth as well as the effects the cooling has on the fatigue and residual stress without machining the weld before the experiments. In general, the impact the cooling has on the fatigue and residual stress should also be studied more, especially because in this study, the fatigue strength specimens were machined and sanded in a way that eliminated the weld geometrical factors.

Today, preheating blankets are used in some situations, and it could be worthwhile to study the feasibility of using the same heat sinks for heating as well. This could be done by switching the water coolant to some other medium that could be used to preheat the steel before the weld and then, for example, by switching back to water to cool the weld afterwards.

References

[1] J. Nowacki, A. Sajek, and P. Matkowski, “The influence of welding heat input on the microstructure of joints of S1100QL steel in one-pass welding,” *Arch. Civ. Mech. Eng.*, vol. 16, no. 4, pp. 777–783, 2016, doi: 10.1016/j.acme.2016.05.001.

[2] F. Javidan, A. Heidarpour, X.-L. Zhao, C. R. Hutchinson, and J. Minkkinen, “Effect of weld on the mechanical properties of high strength and ultra-high strength steel tubes in fabricated hybrid sections,” *Eng. Struct.*, vol. 118, pp. 16–27, 2016, doi: 10.1016/j.engstruct.2016.03.046.

[3] X. Qiang, X. Jiang, F. S. K. Bijlaard, and H. Kolstein, “Mechanical properties and design recommendations of very high strength steel S960 in fire,” *Eng. Struct.*, vol. 112, pp. 60–70, 2016, doi: https://doi.org/10.1016/j.engstruct.2016.01.008.

[4] M. L. Romero, C. Ibañez, A. Espinos, J. M. Portolés, and A. Hospitaler, “Influence of Ultra-high Strength Concrete on Circular Concrete-filled Dual Steel Columns,” *Structures*, vol. 9, pp. 13–20, 2017, doi: 10.1016/j.istruc.2016.07.001.

[5] M. Amraei, T. Skriko, T. Björk, and X.-L. Zhao, “Plastic strain characteristics of butt-welded ultra-high strength steel (UHSS),” *Thin-Walled Struct.*, vol. 109, pp. 227–241, 2016, doi: 10.1016/j.tws.2016.09.024.

[6] P. Markku, “The effects of welding heat input on the usability of high strength steels in welded structures,” Ph.D. dissertation, Dept. Mech. Eng., LUT., Lappeenranta, Finland, 2013.

[7] P. H. M. Hart, “The influence of vanadium-microalloying on the weldability of steels,” *Weld. Cutting*, vol. 4, pp. 204–210, 2003.

[8] S. Kumar, S. K. Nath, and V. Kumar, “Continuous cooling transformation behavior in the weld coarse grained heat affected zone and mechanical properties of Nb-microalloyed and HY85 steels,” *Meter. Des.*, vol. 90, pp. 177–184, 2016, doi: 10.1016/j.matdes.2015.10.071.

[9] Thyssenkrupp, “FB-W Product information for ferritic-bainitic phase steels,” 2016. [Online]. Available: https://www.thyssenkrupp-steel.com/media/content_1/publikationen/produktinformationen/fb_w/thyssenkrupp_fb-w_product_information_steel_en_08-2016_01.pdf

[10] H. K. D. H. Bhadeshia and S. R. Honeycombe, Eds., “The Bainite Reaction,” in *Steels: Microstructure and Properties*, 3rd ed. Oxford, UK: Butterworth-Heinemann, 2006, ch. 6, pp. 129–154.

[11] S. Samanta, P. Biswas, and S. B. Singh, “Analysis of the kinetics of bainite formation below the MS temperature,” *Scr. Mater.*, vol. 136, pp. 132–135, 2017, doi: 10.1016/j.scriptamat.2017.04.030.

[12] S. Samanta, P. Biswas, S. Giri, S. B. Singh, and S. Kundu, “Formation of bainite below the MS temperature: Kinetics and crystallography,” *Acta Mater.*, vol. 105, pp. 390–403, 2016, doi: 10.1016/j.actamat.2015.12.027.

[13] L. C. Chang and H. K. D. H. Bhadeshia, “Microstructure of lower bainite formed at large undercoolings below bainite start temperature,” *Mater. Sci. Technol.*, vol. 12, no. 3, pp. 233–236, 1996, doi: 10.1179/mst.1996.12.3.233.

[14] H. Bhadeshia, *Bainite in steel*. London, UK: IOM communications, 2001.

[15] K. Abbaszadeh, H. Saghafian, and S. Kheirandish, “Effect of Bainite Morphology on Mechanical Properties of the Mixed Bainite-martensite Microstructure in D6AC Steel,” *J Mater Sci Technol*, vol. 28, no. 4, pp. 336–342, 2012, doi: 10.1016/S1005-0302(12)60065-6.

[16] S. B. Singh and H. K. D. H. Bhadeshia, “Estimation of bainite plate-thickness in low-alloy steels,” *Mater. Sci. Eng. A*, vol. 245, no. 1, pp. 72–79, 1998, doi: 10.1016/S0921-5093(97)00701-6.

[17] G. Krauss, *Steels: Processing, Structure, and Performance*, 2nd ed., Ohio, USA: ASM International, 2015.

[18] B. Guo, L. Fan, Q. Wang, Z. Fu, Q. Wang, and F. Zhang, “The Role of the Bainitic Packet in Control of Impact Toughness in a Simulated CGHAZ of X90 Pipeline Steel,” *Metals*, vol. 6, no. 11. 2016, doi: 10.3390/met6110256.

[19] J. Verhoeven, *Steel Metallurgy for the Non-Metallurgist*, Ohio, USA: ASM International, 2007.

[20] H. K. D. H. Bhadeshia and S. R. Honeycombe, Eds., “Formation of Martensite,” in *Steels: Microstructure and Properties*, 3rd ed. Oxford, UK: Butterworth-Heinemann, 2006, ch. 5, pp. 95–128

[21] T. Maki, "Morphology and substructure of martensite in steels," in Phase Transformations in Steels, vol. 2, Diffusionless Transformations, High Strength Steels, Modelling and Advanced Analytical Techniques, E. Pereloma and D. V. Edmonds, Eds. Cambridge, UK: Woodhead Publishing Limited, 2012, ch. 2, pp. 34–58.

[22] Arcelormittal, “A22 - Amstrong Ultra - Ultra High Strength Steels” arcelormittal.com. https://industry.arcelormittal.com/catalogue/A22/EN (accessed Dec. 3, 2020)

[23] S. Endo, N. Ishikawa, J. Kondo, N. Suzuki, and K. Omata, “Advance in high performance linepipes with respect to strength and deformability,” *Proceeding Int. Conf. Pipe Dreamer’s Conf.*, pp. 7–8, 2002.

[24] SSAB, “WeldCalc - The third generation,” 2020. [Online]. Available: https://www.ssab.com/support/calculators-and-tools/weldcalc

[25] SSAB, “Welding of Strenx,” 2018. [Online]. Available: https://www.ssab.com/%20products/brands/strenx/products/strenx-960?%20accordion=workshop&accordion=workshop

[26] Welding – Recommendations for welding metallic materials – Part 1: General guidance for arc welding, EN 1011-1, 2009

[27] Welding – Recommendations for welding metallic materials – Part 2: Arc welding of ferritic steels, EN 1011-2, 2001

[28] L. Lan, X. Kong, C. Qiu, and D. Zhao, “Influence of microstructural aspects on impact toughness of multi-pass submerged arc welded HSLA steel joints,” *Mater. Des.*, vol. 90, pp. 488–498, 2016, doi: 10.1016/j.matdes.2015.10.158.

[29] X. L. Wang, X. M. Wang, C. J. Shang, and R. D. K. Misra, “Characterization of the multi-pass weld metal and the impact of retained austenite obtained through intercritical heat treatment on low temperature toughness,” *Mater. Sci. Eng. A*, vol. 649, pp. 282–292, 2016, doi: 10.1016/j.msea.2015.09.030.

[30] J. H. Kim and E. P. Yoon, “Notch position in the HAZ specimen of reactor pressure vessel steel,” *J. Nucl. Mater.*, vol. 257, no. 3, pp. 303–308, 1998, doi: 10.1016/S0022-3115(98)00451-6.

[31] X. L. Wang *et al.*, “Effect of interpass temperature on the microstructure and mechanical properties of multi-pass weld metal in a 550-MPa-grade offshore engineering steel,” *Weld. World*, vol. 61, no. 6, pp. 1155–1168, 2017, doi: 10.1007/s40194-017-0498-x.

[32] Y. Peng, A. H. Wang, H. J. Xiao, and Z. L. Tian, “Effect of Interpass Temperature on Microstructure and Mechanical Properties of Weld Metal of 690 MPa HSLA Steel,” *Mater. Sci. Forum*, vol. 706–709, pp. 2246–2252, 2012, doi: 10.4028/www.scientific.net/MSF.706-709.2246.

[33] R. Singh, “Chapter 3 - Welding and Joining Processes,” *Applied Welding Engineering (Second Edition)*. Butterworth-Heinemann, pp. 163–195, 2016, doi: 10.1016/B978-0-12-804176-5.00015-3.

[34] I. Bunaziv, O. M. Akselsen, J. Frostevarg, and A. F. H. Kaplan, “Laser-arc hybrid welding of thick HSLA steel,” *J. Mater. Process. Technol.*, vol. 259, pp. 75–87, 2018, doi: 10.1016/j.jmatprotec.2018.04.019.

[35] M. Nilsen, F. Sikström, A.-K. Christiansson, and A. Ancona, “Vision and spectroscopic sensing for joint tracing in narrow gap laser butt welding,” *Opt. Laser Technol.*, vol. 96, pp. 107–116, 2017, doi: 10.1016/j.optlastec.2017.05.011.

[36] Fronius, “CMT - Cold metal transfer: The cold welding process for premium quality,” fronius.com. https://www.fronius.com/en/welding-technology/our-expertise/welding-processes/cmt (acessed Dec. 1, 2019)

[37] ESAB, “The ice advantage,” ESAB.com. https://www.esab.ae/ae/en/automation/process-solutions/saw/saw-ice/index.cfm (accessed Dec. 1, 2019)

[38] J. T. Bono, J. N. DuPont, D. Jain, S.-I. Baik, and D. N. Seidman, “Investigation of Strength Recovery in Welds of NUCu-140 Steel Through Multipass Welding and Isothermal Post-Weld Heat Treatments,” *Metall. Mater. Trans. A Phys. Metall. Mater. Sci.*, vol. 46, no. 11, pp. 5158–5170, 2015, doi: 10.1007/s11661-015-3087-x.

[39] H. Xie, L.-X. Du, J. Hu, G.-S. Sun, H.-Y. Wu, and R. D. K. Misra, “Effect of thermo-mechanical cycling on the microstructure and toughness in the weld CGHAZ of a novel high strength low carbon steel,” *Mater. Sci. Eng. Struct. Mater. Prop. Microstruct. Process.*, vol. 639, pp. 482–488, 2015, doi: 10.1016/j.msea.2015.05.033.

[40] S. Kim, D. Kang, T.-W. Kim, J. Lee, and C. Lee, “Fatigue crack growth behavior of the simulated HAZ of 800MPa grade high-performance steel,” *Mater. Sci. Eng. A*, vol. 528, no. 6, pp. 2331–2338, 2011, doi: 10.1016/j.msea.2010.11.089.

[41] X. Chen, B. Liao, G. Qiao, Y. Gu, X. Wang, and F. Xiao, “Effect of Nb on Mechanical Properties of HAZ for High-Nb X80 Pipeline Steels,” *J. Iron Steel Res. Int.*, vol. 20, no. 12, pp. 53–60, 2013, doi: 10.1016/S1006-706X(13)60216-2.

[42] J. Jang, B.-W. Lee, J.-B. Ju, D. Kwon, and W. Kim, “Experimental analysis of the practical LBZ effects on the brittle fracture performance of cryogenic steel HAZs with respect to crack arrest toughness near fusion line,” *Eng. Fract. Mech.*, vol. 70, no. 10, pp. 1245–1257, 2003, doi: 10.1016/S0013-7944(02)00111-X.

[43] C. L. Davis and J. E. King, “Cleavage initiation in the intercritically reheated coarse-grained heat-affected zone: Part I. Fractographic evidence,” *Metall. Mater. Trans. A*, vol. 25, no. 3, pp. 563–573, 1994, doi: 10.1007/BF02651598.

[44] W. Jiang, Y. Zhang, and W. Woo, “Using heat sink technology to decrease residual stress in 316L stainless steel welding joint: Finite element simulation,” *Int. J. Press. Vessel. Pip.*, vol. 92, pp. 56–62, 2012, doi: 10.1016/j.ijpvp.2012.01.002.

[45] H. Myllymäki, “Hitsausenergian hallinta korkealujuusteräksillä eri hitsausasennoissa,” B.S. thesis, Dept. Civ. Eng., HAMK, Hämeenlinna, Finland 2015.

[46] J. Gabzdyl, “Cryogenic weld cooling.” industrial-lasers.com. https://www.industrial-lasers.com/welding/article/16485270/cryogenic-weld-cooling (accessed Dec. 3, 2020).

[47] C. L. Jenney and A. O’Brien, Eds., Welding Science and Technology in Welding Handbook, vol. 1, 9th ed. Miami, FL, USA: American Welding Society, 1991.

[48] M. D. Chapetti and L. F. Jaureguizahar, “Fatigue behavior prediction of welded joints by using an integrated fracture mechanics approach,” *Int. J. Fatigue*, vol. 43, pp. 43–53, 2012, doi: 10.1016/j.ijfatigue.2012.02.004.

[49] T. Björk, J. Samuelsson, and G. Marquis, “The Need for a Weld Quality System for Fatigue Loaded Structures,” *Weld. World*, vol. 52, no. 1, pp. 34–46, 2008, doi: 10.1007/BF03266615.

[50] A. F. Hobbacher, “Recommendations for Fatigue Design of Welded Joints and Components, Doc. XIII-2151-07/XV-1254-07.” International Institute of Welding, Paris, France, 2007.

[51] Ruukki, “Optim MC structural steel.” Ruukki.com. http://www.ruukki.com/Steel/Hot- rolled-steels/Structural-steels/Optim-MC-structural-steel (accessed Jul. 1, 2016).

[52] SSAB, “Strenx 960 - High-Strength S960QL Structural Steel.” SSAB.com. http://www.ssab.com/products/brands/strenx/products/strenx-960 (accessed Jun. 6, 2017).

[53] SSAB, “Strenx 960 MC - High-strength structural steel at 960 MPa.” SSAB.com. http://www.ssab.com/products/brands/strenx/products/strenx-960-mc (accessed Jun. 6, 2017).

[54] SSAB, “Strenx 700 MC Plus.” SSAB.com. https://www.ssab.com/products/brands/strenx/products/strenx-700-mc-plus (accessed Feb. 4, 2019).

[55] Force controlled constant amplitude axial fatigue testing of metallic materials, ASTM E 466, 2015

[56] R. Rabb, *Väsyminen ja todennäköisyysteoria*. Oulu, Finland: University of Oulu, 2017.

[57] R.L. Brockenbrough Associates, INC "Effect of Yield-Tensile Ratio on Structural Behavior – High Performance Steels for Bridge Construction," Steel Market Development Institute. 1995.

[58] A. C. Bannister, "Yield stress/tensile stress ratio: results of experimental programme ," British steel, Rotherham, United Kingdom, 1999. [Online]. Available: www.eurofitnet.org/sintap_BRITISH_STEEL_BS-25.pdf

[59] X. L. Wang, Y. R. Nan, Z. J. Xie, Y. T. Tsai, J. R. Yang, and C. J. Shang, "Influence of welding pass on microstructure and toughness in the reheated zone of multi-pass weld metal of 550MPa offshore engineering steel," *Mater. Sci. Eng. A*, vol. 702, pp. 196–205, 2017, doi: 10.1016/j.msea.2017.06.081.

[60] J. Li, C. Zhang, and Y. Liu, "Influence of carbides on the high-temperature tempered martensite embrittlement of martensitic heat-resistant steels," *Mater. Sci. Eng. A*, vol. 670, pp. 256–263, 2016, doi: 10.1016/j.msea.2016.06.025.

[61] G. F. Sun *et al.*, "Microstructure and mechanical properties of HSLA-100 steel repaired by laser metal deposition," *Surface and Coatings Technology*, vol. 351. pp. 198–211, 2018, doi: 10.1016/j.surfcoat.2018.07.048 ".

[62] H. Kyung Sung, D. Ho Lee, S. Yong Shin, S. Lee, J. Yong Yoo, and B. Hwang, "Effect of finish cooling temperature on microstructure and mechanical properties of high-strength bainitic steels containing Cr, Mo, and B," *Mater. Sci. Eng. A*, vol. 624, pp. 14–22, 2015, doi: 10.1016/j.msea.2014.11.035.

Original publications

I Laitila, J., Larkiola, J., & Porter, D. (2017). Effect of forced cooling on the tensile properties and impact toughness of the coarse-grained heat-affected zone of a high-strength structural steel. *Welding in the World*, *62*(1), 79–85. https://doi.org/10.1007/s40194-017-0532-z

II Laitila, J., Larkiola, J., & Porter, D. (2018). Effect of forced cooling after welding on CGHAZ mechanical properties of a martensitic steel. *Welding in the World*, *62*(6), 1247–1254. https://doi.org/10.1007/s40194-018-0617-3

III Laitila, J., Larkiola, J., & Porter, D. (2019). Effect of heat sinks on cooling time to weld interpass temperature. *MATEC Web of Conferences*, *269*, 01007. https://doi.org/10.1051/matecconf/201926901007

IV Laitila, J., & Larkiola, J. (2019). Effect of enhanced cooling on mechanical properties of a multipass welded martensitic steel. *Welding in the World*, *63*(3), 637–646. https://doi.org/10.1007/s40194-018-00689-7

V Laitila, J., Keränen, L. & Larkiola, J. (2020). Effect of enhanced weld cooling on the mechanical properties of a structural steel with a yield strength of 700 MPa. *SN Applied Sciences, 2*, 1888. https://doi.org/10.1007/s42452-020-03695-x

Original publications are not included in the electronic version of the dissertation.

758. Miettinen, Jyrki & Visuri, Ville-Valtteri & Fabritius, Timo (2020) Chromium-, copper-, molybdenum-, and nickel-containing thermodynamic descriptions of the Fe–Al– Cr–Cu–Mn–Mo–Ni–Si system for modeling the solidification of steels

759. Alasalmi, Tuomo (2020) Uncertainty of classification on limited data

760. Kinnunen, Hannu (2020) Studies for the development, validation, and application of wearable technology in the assessment of human health-related behavior

761. Abou Zaki, Nizar (2020) The role of agriculture expansion in water resources depletion in central Iran

762. Gyakwaa, Francis (2020) Application of Raman spectroscopy for the characterisation of synthetic non-metallic inclusions found in Al-killed calcium treated steels

763. Pandya, Abhinay (2020) Demographic inference and affect estimation of microbloggers

764. Eckhardt, Jenni (2020) Mobility as a Service for public-private partnership networks in the rural context

765. Apilo, Olli (2020) Energy efficiency analysis and improvements of MIMO cellular communications

766. Gogoi, Harshita (2020) Development of biosorbents for treatment of industrial effluents and urban runoffs

767. Saavalainen, Paula (2020) Sustainability assessment tool for the design of new chemical processes

768. Ferdinando, Hany (2020) Classification of ultra-short-term ECG samples : studies on events containing violence

769. Leinonen, Marko (2020) Over-the-air measurements, tolerances and multiradio interoperability on 5G mmW radio platform

770. Pakkala, Daniel (2020) On design and architecture of person-centric digital service provisioning : approach, fundamental concepts, principles and prototypes

771. Mustaniemi, Janne (2020) Computer vision methods for mobile imaging and 3D reconstruction

772. Khan, Uzair Akbar (2020) Challenges in using natural peatlands for treatment of mining-influenced water in a cold climate : considerations for arsenic, antimony, nickel, nitrogen, and sulfate removal

773. Kumar, Tanesh (2020) Secure edge services for future smart environments

Book orders:
Virtual book store
http://verkkokauppa.juvenesprint.fi

UNIVERSITY OF OULU P.O. Box 8000 FI-90014 UNIVERSITY OF OULU FINLAND

ACTA UNIVERSITATIS OULUENSIS

ISBN 978-952-62-2814-3 (Paperback)
ISBN 978-952-62-2815-0 (PDF)
ISSN 0355-3213 (Print)
ISSN 1796-2226 (Online)

UNIVERSITY OF OULU